RSC Advances

REVIEW

View Article Online
View Journal | View Issue

Cite this: *RSC Adv.*, 2022, **12**, 5891

Identifying surface degradation, mechanical failure, and thermal instability phenomena of high energy density Ni-rich NCM cathode materials for lithium-ion batteries: a review

Fikadu Takele Geldasa, [a] Mesfin Abayneh Kebede, *[bd] Megersa Wodajo Shura [a] and Fekadu Gashaw Hone *[c]

Among the existing commercial cathodes, Ni-rich NCM are the most promising candidates for next-generation LIBs because of their high energy density, relatively good rate capability, and reasonable cycling performance. However, the surface degradation, mechanical failure and thermal instability of these materials are the major causes of cell performance decay and rapid capacity fading. This is a huge challenge to commercializing these materials widely for use in LIBs. In particular, the thermal instability of Ni-rich NCM cathode active materials is the main issue of LIBs safety hazards. Hence, this review will recapitulate the current progress in this research direction by including widely recognized research outputs and recent findings. Moreover, with an extensive collection of detailed mechanisms on atomic, molecular and micrometer scales, this review work can complement the previous failure, degradation and thermal instability studies of Ni-rich NMC. Finally, this review will summarize recent research focus and recommend future research directions for nickel-rich NCM cathodes.

Received 16th November 2021
Accepted 10th February 2022

DOI: 10.1039/d1ra08401a

rsc.li/rsc-advances

[a]*Adama Science and Technology University, Department of Applied Physics, P. O. Box 1888, Adama, Ethiopia*

[b]*Energy Centre, Smart Places, Council for Scientific and Industrial Research (CSIR), Pretoria 0001, South Africa. E-mail: mkebede@csir.co.za*

[c]*Addis Ababa University, Department of Physics, P. O. Box: 1176, Addis Ababa, Ethiopia. E-mail: fekeye@gmail.com*

[d]*Molecular Sciences Institute, School of Chemistry, University of the Witwatersrand, Johannesburg 2050, South Africa*

Fikadu Takele was born in Welega, Ethiopia, in 1993. He received his BSc degree in Applied Physics from Hawassa University in 2015 and his MSc degree in Solid State Physics from Dilla University, in 2017. Currently he is a PhD student at Adama Science and Technology University under the supervision of Dr Fekadu Gashaw, Dr Mesfin Abayneh and Dr Megersa Wodajo. His research interest is on energy storage electrode materials specifically on lithium ion batteries.

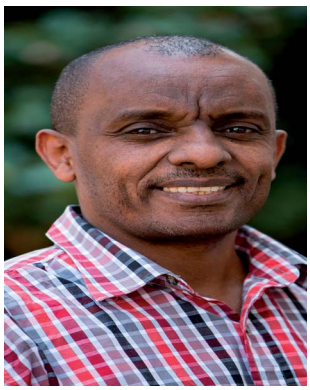

Mesfin Kebede obtained his PhD in Metallurgical Engineering/Applied Physics from Inha University, South Korea. He is currently a Principal Research Scientist at the Energy Centre of Council for Scientific and Industrial Research (CSIR), South Africa. In addition, he holds a Honorary Associate Professor position at the University of the Witwatersrand, South Africa. His current research mainly focuses on the development and characterization of electrode materials for energy storage and fabrication of coin cells and pouch cells for full cells and improving the electrochemical performance of electrode materials for energy storage systems such as lithium-ion batteries, sodium-ion batteries, and supercapacitors.

1 Introduction

Today's electricity generation and transportation depend heavily on fossil fuels, thus becoming the two major sources of CO_2 emissions that lead to global warming.[1] Ecofriendly renewable energy sources such as wind and solar must be increasingly used to reduce or eliminate fossil fuel utilisation.[2,3] The energy produced by these renewable energies must be stored and due to their power and energy density greatly exceeding those of other battery systems lithium-ion batteries (LIBs) are the most preferred energy storage devices.[4–6] Compared to conventional secondary batteries, LIBs are advantageous in terms of low environmental pollution, high energy density, good rate performance, and long cycle life.[7] LIBs have been used successfully in a variety of applications, from portable electronics and electric vehicles (EVs) to energy storage systems.[8] Fig. 1a[9] shows the relationship between specific energy density and volumetric energy density for the different rechargeable battery technologies. Specifically, the general goal of battery development technology is to increase energy and power densities, while minimizing volumetric and mass constraints (*i.e.*, move to the upper right of Fig. 1a).[9]

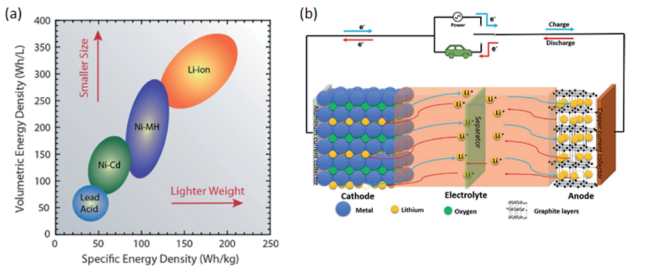

Fig. 1 (a) Diagram comparing the rechargeable battery technologies as a function of volumetric and specific energy densities. The arrows indicate the direction of development to reduce battery size and weight.[9] (b) Schematic diagram of the charge/discharge principle of a LIB cell.[10]

Historically, the lithium-based rechargeable battery was first demonstrated in the 1970s, which was proposed by M. S. Whittingham while working at Exxon in 1976.[11] Apparently, LIBs have two different current collectors, two electrodes (anode and cathode), and the separator/electrolyte main components, and Whittingham's battery was made with layered TiS_2 as the cathode and Li metal as the anode. The positive cathode worked well, whereas the lithium metal anode was shown to have uneven dendrite growth during charging and discharging.[11] Apparently dendrite is the main enemy of LIBs, it could penetrate the separation layer and reach the opposite electrode, resulting in a short circuit and a potential fire hazard.[12] The dendrite growth of Whittingham's battery was proved difficult to solve, and the commercialization of such type of batteries became a failure. Because of this safety problem, researchers have increasingly proposed for both electrodes that can accommodate ions. In 1980 John B. Goodenough and his co-workers at Oxford University, UK, discovered the layered Li_x-CoO_2 cathode materials.[8,9,13] Due to the absence of suitable anode materials and electrolytes that match the discovered positive electrode, it took nearly ten years to commercialize LIBs.[7] That is, the lack of safe anode materials limited the application of layered oxide cathode $LiCoO_2$ in LIBs.[14] In 1980, Rachid Yazami examined lithium intercalation compounds in graphite and discovered the graphite anode.[15]

In the early 1980s, Akira Yoshino conceived the LIB and he completed a practical prototype in 1986.[16] He replaced the negative electrode with carbon that provided greater capacity without causing decomposition of the electrolyte. The secondary battery that he successfully fabricated consist carbon coke as anode and $LiCoO_2$ as cathode and enabled stable charging and discharging over many cycles for a long period. Yoshino also carried out the first safety test on LIBs to validate their enhanced safety features, by dropping iron lumps on the

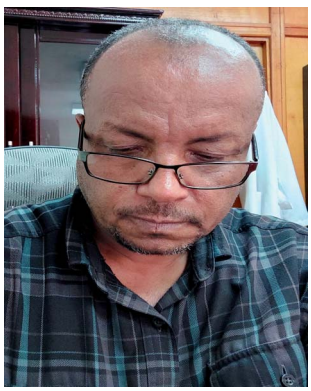

Megersa Wodajo Shura earned his BSc degree in Physics at Asmara University, Eritrea in 1990. After serving at different institutions for a while, he joined Addis Ababa University for his MSc Study in 1997. Then, he joined Adama Teachers College until he moved to Adama Science and Technology University in September 2006. Then, he joined Nelson Mandela University, South Africa for his PhD study in March 2009. Upon completion of his PhD, he returned to ASTU and served as an Assistance and Associate Professor of Physics. His research interest is dealing with the various optoelectrical properties of inorganic semiconductors.

Fekadu Gashaw is an Associate Professor of Materials Physics and is currently working at Addis Ababa University Department of Physics as a researcher and lecturer. He obtained his first degree in Physics from Debub University in 2001 and his MSc degree from AAU in Laser Spectroscopy (2006). He got his PhD degree from KNUST (Ghana) (2015). Fekadu was also a postdoctoral researcher at the University of the Free State, (South Africa) from 2016 to 2020. His research mainly focuses on the development and characterization of novel nanomaterials for various applications such as energy storage and conversion, gas sensors and antimicrobial activities.

battery cells, in contrast to that of metallic lithium batteries which caused fire and explosion. Based on these effective efforts, the first commercial LIB was released by Sony company in 1991.[17] LIB commercialized by Sony is still governing of the electronic market today.[7] Moreover, the commercialization of LIB was successful by the effort of the three scientists Whittingham, Goodenough, and Yoshino. To acknowledge their pioneering contribution, they were awarded the 2019 Nobel Prize in Chemistry.[18]

(Fig. 1b)[10] shows the working principle of the LIBs cell consisting of graphite as an anode and layered lithium oxide as cathode materials. The full cell battery undergoes both discharge and charge processes. On charging, Li-ions are moving from the cathode to anode through electrolyte and electrons flow through an external circuit to anode. On discharging, electrons are moving from the anode through the copper current collector and, simultaneously, Li-ion extracted from the anode into the electrolyte and migrates toward the cathode. Then, the removed electron enters the cathode from an external circuit through the aluminum current collector. Discharging process is a spontaneous process, whereas charging needs external power sources and is non-spontaneous.

Currently, LIBs have been successfully applied in portable electronics, but researchers need them to electrify the world. However, conventional LIBs could not meet the required capacity to electrify the world.[19] Especially, compared to the anode material, the cathode material capacity is lower, which greatly hinders the further development of LIBs.[20] Therefore, to improve energy storage materials, researchers around the world are trying to improve the capacity of existing cathode materials and discovering new cathode materials. More recently, LIBs have been considered to be the most promising energy storage devices for electric vehicles (EVs) and have been used by Nissan (Leaf) and Tesla to manufacture electric vehicles.[19,20] For the sake of environmental protection and energy conservation, electric vehicles are considered as the future means of transportation, which do not emit pollutants and can efficiently utilize energy.[21,22] Despite their environmental advantages, electric vehicles have limited popularity due to inferior battery performance and higher cost compared to vehicles with internal combustion engine.[20] For more development of EVs and their market-dominant, LIBs having high energy density, long life, good safety, fast charging, and low price are needed. In this sense, EV batteries require cathode materials with high energy density to achieve these properties because the most commonly used anode, graphite, can deliver a much higher specific capacity (372 mA h g^{-1}) than available cathodes.[19] Because of their high energy density, Ni-rich cathode materials are promising next-generation batteries both for the improvement of portable electronics and for the development of EVs. Ni-rich cathodes can be either nickel–cobalt–manganese (NCM) or nickel–cobalt–aluminum (NCA) which has similar crystal structures.[23] However, these cathode materials are commercialized currently still there are remaining challenges in cycle life, surface degradation and thermal stability that hindered them from widely used for EVs. Thus, LIBs and LIB-based systems can fail catastrophically causing fire and/or explosion, while it is important to gain an understanding of the energetics and dynamics of such failure causes to mitigate their future occurrence.[24] So, before trying to solve these challenges, it is more important to understand the mechanisms of these challenges. Many review papers have been published on the degradation mechanisms of Ni-rich cathode materials. However, to the best of our knowledge, there is no reported review article emphasized on the well organized and identified surface degradation, mechanical failure and thermal instability of Ni-rich NCM cathode materials, specifically including upper cutoff voltage. The challenges discussed in this review are also dependent on each other but not extremely identified by scientific investigation. In this paper, we present a comprehensive review to summarized related research out puts on NCMs challenges as well as how either of the three degradation mechanisms focused in this review affect one another. Hence, we believe that this review could provide an overall understanding for researchers interested in the currently hot issue of the degradation mechanisms of Ni-rich cathode materials and finding well-developed mitigation strategies for these challenges.

2 Cathode materials

Based on the discovery of John B. Goodenough and successfully charged/discharged over many cycles, $LiCoO_2$ became the primary successfully used positive electrode in LIBs. It has excellent electrochemical performance; however, it poses some problems, such as safety, environmental hazard, and high cost, because of the limited availability of cobalt. During charging, when half of the Li-ions are removed from the host structure, the structural stability of $LiCoO_2$ rapidly deteriorates and researchers improved its cycle performance by limiting the cut-off voltage, which delivers only about 140 mA h g^{-1} capacity, which is half of the theoretical capacity.[7] Other researchers have approximated this value for commercial $LiCoO_2$ to 165 mA h g^{-1} out of a high theoretical specific capacity of 274 mA h g^{-1}, due to its significant structural instability and severe capacity fading at voltages greater than 4.35 V *vs.* Li/Li^+.[25] Also, it could not meet the required energy and power density, especially, for electric vehicles. To solve these issues, Co must be partially or fully replaced by cheap and non-toxic elements. Additionally, the electrochemical performance, price, and safety of LIBs are mainly dependent on cathode materials, it is important to look for materials with high energy density, cheap, and safe.[21,22]

After the discovery of the layered structure $LiCoO_2$ in 1980, other positive electrodes such as the $LiMn_2O_4$ spinel structure in 1986 and the $LiMPO_4$ (M = Fe, Mn, *etc.*) olivine family in 1997 have been discovered.[26] The spinel-phase $LiMn_2O_4$ is the lowest cost, environmental friendliness, and naturally abundant materials, but it exhibits the problem of Mn^{2+} ion dissolution, which causes the capacity fading and limits its development.[27] Olivine $LiFePO_4$ is another positive electrode material with low cost, excellent electrochemical properties, great thermal stability, and non-toxicity.[7] This positive electrode has low Li-ion diffusion, poor conductivity, and poor charge/discharge rate performance. Many researchers have endeavored to

resolve these problems, but the discharge platform of $LiFePO_4$ is approximately around 3.4 V and its theoretical specific capacity is 170 mA h g^{-1}.[28] Including the aforementioned positive electrodes different layered materials such as $LiNiO_2$, $LiMnO_2$, *etc.* have been discovered.[29] $LiNiO_2$ has the same structure as $LiCoO_2$ and high energy density and low cost; however, at high temperature or high voltage, it exhibits poor structural stability and low cycle reversible, which limits its development.[27] The structure and potential profiles of the olivine, spinel, and different layered cathode materials during discharge are shown in (Fig. 2a).[30] Because of the drawback of all of the aforementioned cathode materials, the development of LIBs continued and many improvements and alternatives have been reported. Researchers around the world have endeavored to develop a further increasing energy density and reducing the cost of electrode materials, particularly cathode materials, which are still a limiting factor on the total energy density of LIBs and occupy a great weight of LIB cell components (Fig. 2b).[31,32] They are mainly aimed at discovering a rechargeable battery with high specific capacity, lower cost, environmental friendliness, and fast charging for transportation and energy storage in addition to for portable electronics.[33] Recently, the layered oxide materials, which consist of ternary transition materials, are becoming promising cathode materials. Although single component layered cathode materials, including $LiNiO_2$ and $LiMnO_2$, also suffer from intrinsic problems such as poor cyclability and rate capability, as well as complexity in preparation, layered oxide nickel–cobalt–manganese (NCM) or nickel–cobalt–aluminum (NCA) exhibited promising electrochemical properties, which vary depending on the composition of transition metals (TMs) in the structure.[34] Layered oxide nickel–cobalt–manganese (NCM) is a very sensitive area of today's LIBs studies. They can be represented as $LiNi_xCo_yMn_zO_2$ with different compositions of TMs. TMs in NCM cathode materials play different roles in terms of crystal structure and electrochemical properties. Generally, Ni provides the majority of the reversible capacity by converting Ni^{2+} to Ni^{3+}/Ni^{4+}, while Co offers good electronic conductivity and reinforces layered ordering with improved rate capability and additional capacity derived from the $Co^{3+/4+}$ redox reaction (by converting Co^{3+} to Co^{4+}). Furthermore, Mn stabilizes the local structure to achieve steady cycling performance, although Mn remains electrochemically inert in the tetravalent state during the charge–discharge process.[27] Consequently, the intrinsic structure and performance of $LiNi_xCo_yMn_zO_2$ strongly depend on the compositional ratio of Ni, Co, and Mn.[19]

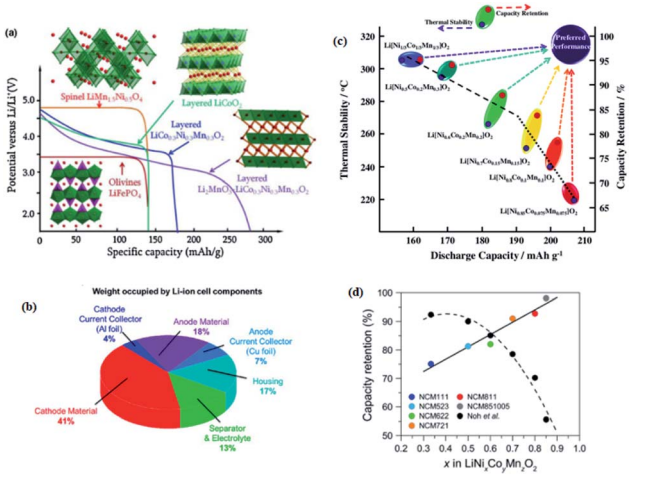

Fig. 2 (a) Li-ion battery cathodes: important formulae, structures, and potential profiles during discharge[30] (b) chart showing the weight fraction occupied by the components of a commercial lithium-ion battery cell.[31,32] (c) A map of relationship between discharge capacity, and thermal stability and capacity retention of $Li/Li[Ni_xCo_yMn_z]O_2$ (x = 1/3, 0.5, 0.6, 0.7, 0.8 and 0.85).[35] (d) Comparison of the capacity retention after 100 cycles achieved by tailoring U_{max}.[36]

After Ohzuku and Makimura reported $LiNi_{1/3}Co_{1/3}Mn_{1/3}O_2$ (NCM111), NCM-based LIBs have become the mainstream with gradual improvements in NCM technology through the steady increase in nickel content in each generation of cathode materials.[37] Compared to $LiCoO_2$, $LiMn_2O_4$, and $LiNiO_2$, NCM-based materials have outstanding electrochemical properties, such as high energy density, high reversibility, good environmental compatibility, and excellent charge/discharge rate.[38] For Ni-rich cathode materials, the nickel content in NCM-based materials exceeds Co and Mn content, which is above 50%.[27,28] The theoretical capacity of conventional cathode materials is 170 mA h g^{-1} for olivine $LiFePO_4$, 140 mA h g^{-1} for spinel $LiMn_2O_4$, 140–160 mA h g^{-1} for layered $LiCoO_2$ and these materials are limited by their insufficient capacity, which cannot meet the increasing requirements for practical applications.[39] The main advantage of Ni-rich materials is their high discharge capacity (200–220 mA h g^{-1}), which represents a large increase in energy density (~800 W h kg^{-1}) as compared to conventional $LiCoO_2$ (~570 W h kg^{-1}) and $LiMn_2O_4$ spinel (~440 W h kg^{-1}) materials.[28,33] In addition, the enhancement of the capacity of LIBs can be achieved by increasing the Ni content. In the composition of NCM cathode materials, as the content of Ni increases, the capacity of the cathode materials also increases. For example, the Ni-rich $LiNi_{0.6}Co_{0.2}Mn_{0.2}O_2$ has a high specific capacity ~170 mA h g^{-1}.[40] When the Ni content increases to $LiNi_{0.8}Co_{0.1}Mn_{0.1}O_2$ a higher specific capacity of 200 mA h g^{-1} is achieved.[41]

Nevertheless, as Ni content increases in layered Ni-rich oxide, some intrinsic problems, such as poor capacity retention and low thermal stability, are revealed. Hyung-Joo Noh *et al.*[35] have investigated the electrochemical and thermal properties of the composition of $LiNi_xCo_yMn_zO_2$ (x = 1/3, 0.5, 0.6, 0.7, 0.8 and 0.85) as a function of the Ni content. They identified that there is a nearly linear decrease in thermal stability and capacity retention as the discharge capacity increases by increasing the relative fraction of Ni in the $LiNi_xCo_yMn_zO_2$ electrodes. As shown in (Fig. 2c),[35] among the tested compositions; the 1/3 cathode exhibited the best capacity retention and thermal stability; however, its discharge capacity was limited due to the low Ni content in the composition. However, the 85% Ni content cathode exhibits severe capacity fading and the worst thermal stability in spite of the large discharge capacity, while the 1/3 electrode showed the highest

safety. However, Lea de Biasi *et al.*[36] have found that Ni-rich NCMs show better capacity retention than those with a low Ni content compared with Hyung-Joo Noh *et al.* in (Fig. 2d),[36] which was achieved by tailoring cut-off voltage (U_{max}), although they have a structural instability. In addition, poor cycle life due to structural instability upon long-term cycling, particularly under high charge voltage (>4.3 V),[42] high defect concentration, and insufficient C-rate performance become more prominent.[27] Not only these, the sensitivity to ambient moisture, the formation of micro-cracks[15,16] and micro-strain[16,18] during cycling, and the thermal instability upon delithiation, which cause capacity fading of Ni-rich oxides have been revealed. Parasitic reactions,[43] cation mixing by leading to restructured surface regions,[44] active material dissolution,[45] and oxygen release[46] are the primary factors responsible for the cathode surface degradation mechanism. The high charge voltage would lead to a severe reaction of the Ni-rich surface with the electrolyte, forming a thick cathode-electrolyte interface (CEI) layer to increase the interfacial resistances of electrodes. In addition, highly oxidized $Ni^{3+/4+}$ ions at deep charge are easily destabilized and reduced as Ni^{2+} ions, resulting in cation migrations to form surface reconstruction layers consisting of spinel-like and/or NiO-like rock salt phases. This surface structure transition considerably increases the kinetic barrier for Li-ion diffusion, leading to capacity degradation.[42] The improved outstanding energy density of Ni-rich cathode material is good while improving cathode structural and thermal stabilities thus safety issues and application range have become the focus of the subsequent research. Many efforts based on different strategies such as dopants, gradient layers, surface coatings, carbon matrixes, and advanced synthesis methods have been devoted so far to improve the electrochemical performance of layered Ni-rich oxide cathode material.[39,47] However, it is very important to understand the degradation mechanisms in order to find effective strategies for the aforementioned challenges and to making better batteries.

3 Challenges in NCM materials

To achieve a sufficiently high specific capacity at a given maximum cut-off voltage, the Ni content in the composition of NCM-based cathode materials must be continuously increased. Thus, in LIBs, energy densities can be significantly increased by the inclusion of more Ni content in the NCM cathode materials.[48] However, due to surface-related chemical degradations and mechanical failures, Ni-rich NCM cathode materials lead to poor cycling stability.[49] The unprotected surface of Ni-rich NCM cathode materials can easily react with electrolyte during battery cycling, causing irreversible structure transformation, composition modification, and surface passivation layer formation, which contribute to capacity decay, and also act as a blocking layer, causing voltage fading. In addition to surface degradation, mechanical failures, such as crack-induced material disintegration, are the major causes of cell performance decay. Mechanical cracks can lead to fragmentations of active materials, which cause poor electronic conduction and exposure of fresh surfaces to electrolytes. Moreover, battery degradation can be occurred during charging, discharging and at rest.[50] At high cut-off voltage, these challenges can be caused, and therefore we start our discussions from the upper cut-off voltage and we will continue to the identification of these challenges and their mechanisms.

3.1 Upper cutoff voltage

High energy density, high power density, low cost, and longer lifetime are required for LIBs to be widely applied in portable electronics, grid storage systems, and electric vehicles. High energy density can be achieved by increasing the upper cutoff voltage in NCM-based LIBs.[20,46] Although the theoretical capacity of NCM is as high as ~275 mA h g^{-1}, not all of the Li^+ can be removed due to the structural instabilities that form when deep Li is removed.[44] For deep Li^+ removal, the upper cutoff voltage must be increased. However, increasing the upper cut-off voltage can increase undesirable side reactions at the electrode/electrolyte interface, surface film formation, and metal dissolution, which ultimately decrease the battery lifetime.[51] For these reasons the operating potential of NCM based cathode materials is limited to approximately 4.3 V; this results in their capacity being much below their theoretical capacity.

Having an improved energy density is the very interesting and required one in LIBs. Lea de Biasi *et al.*[36] have proposed two major strategies to improve the energy density of LIBs using NCM cathode active materials. The first is to increase the content of Ni, which allows larger amounts of Li to be extracted at a given cut-off voltage (U_{max}). The other is to increase U_{max}, for medium Ni content NCM active materials. They have performed electrochemical tests on NCM111, NCM523, NCM622, NCM721, NCM811, and NCM851005 using coin-type cells with a lithium metal counter electrode. The highest Ni content is the more Li extracted, hence the highest the specific capacity. They have also observed that gravimetric energy density (GED) increases with both increasing Ni content and U_{max}.

The origin of faster capacity fading at high cutoff potentials is a complex,[52] however, the H2–H3 phase change is reported as the origin of capacity fading at a high cutoff potential. The advantages, challenges, and origin of the challenges in increasing the upper cutoff in Ni-rich NCM materials are shown in (Fig. 3).

Researchers have investigated the effects of increasing and decreasing of upper cut-off voltages for different Ni-rich NCM cathode materials. Yanli Ruan *et al.*[47] have investigated the electrochemical performance of NCM622 at 4.2 V, 4.5 V, and 4.8 V. They have observed that as the upper cutoff voltage increases the charge/discharge capacity also increases, whereas the capacity retention decreases. The cycling stability of this NCM622 active material strongly depends on the cutoff voltage. The discharge voltage plateaus are almost the same in the first discharge whereas decreases after 100 cycles with increasing upper cut-off voltages. After 100 cycles, the discharge capacity decays as the upper cutoff voltage increases. For 4.2 V, all the capacity degradation after 100 cycles is attributed to the increase in cell impedance, implying that the structure of the NMC622 material can be well maintained in low-voltage cycling.

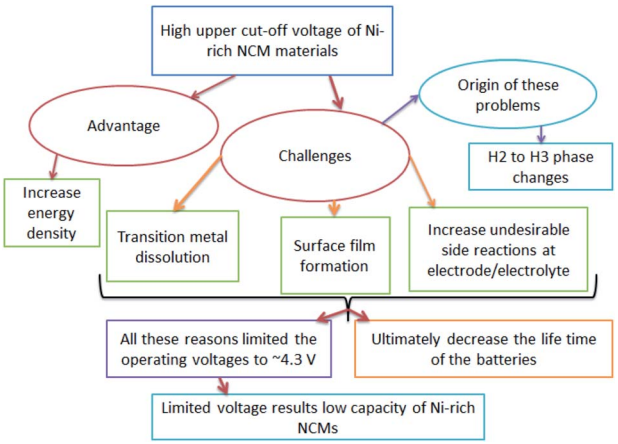

Fig. 3 The flow of the advantages, challenges and origin of increasing upper cut-off voltage in Ni-rich NCM cathodes.

The effects of increasing the upper cut-off voltages on electrochemical properties of Ni-rich NCM cathodes are dependent on the aggregation modes of the primary particles.[53] At a high cutoff voltage, a significant contraction and/or expansion of the lattice parameter vector may exist, which results in the changes in lattice volume. The nonuniform accommodation of such a volume change will generate severe local strain, which might result in mechanical failure and inter-granular cracks.

The charge/discharge cycle of Ni-rich NCM-based materials at high upper cutoff voltage can also cause phase transformations. Sung-Kyun Jung *et al.*[34] have proposed the degradation mechanisms of NCM523 at high voltages by comparing 4.5 V and 4.8 V cutoff voltages (see (Fig. 4)).[34] Cycling at 4.5 V, the electrode surface suffers from a phase transformation mainly to the spinel phase, with a trace of rocksalt phase formation. When the cutoff voltage increases to 4.8 V, then the highly oxidative environment exhibits the formation of the rocksalt phase. As can be seen in (Fig. 4), the rocksalt phase encircles both the rhombohedral and spinel phases, increasing the impedance of the electrode. Roland Jung *et al.*[44] have compared the electrochemical performance of the NCM111, NCM622, and NCM811 electrodes at different cutoff voltages and they concluded from those results as cutoff voltages increase, the capacity increases, and when Ni content increases capacity also increase with increasing cut-off voltages. The average discharge voltages for both NCM111 and NCM622 are very similar. As the Ni content increases to NCM811, due to the less stable cycling behavior of NCM811, the upper cutoff voltage is limited to low voltages and displays a continuously decreasing mean voltage cathode discharge value, even at the lowest cutoff voltage. Therefore, from this report result, as Ni content increases the onset potential decreases.

A differential capacity plot of the delithiation and lithiation of the three NCM materials in NCM-graphite cells of the 3rd cycle is represented in (Fig. 5).[44] This plot investigates the origin of the difference and the reason for the instability for NCM111 and NCM622 at 4.6 V and for NCM811 at 4.1–4.2 V. The voltage region up to 3.8 V is stable for all NCMs, with two anodic peaks between 3.4 V and 3.8 V, which originates from the lithium insertion into the anode and the phase transition from a hexagonal to a monoclinic (H1 → M) lattice of the NCM[54] respectively for the two anodic peaks. In the region above 3.8 V, the differential capacity curve for the NCM811 cell deviates from that of the NCM111 and NCM622 cells. NCM811 has a small anodic feature at ~3.95 V, which belongs to the M → H2 phase transition, and a large anodic peak at ~4.15 V, which belongs to the H2 → H3 phase transition,[48] both of which are not present for the other NCMs. On the contrary, such deviations are not observed for NCM111 and NCM622; however, for NCM622 a broad peak is observed around 4.1 V, which could indicate an M → H2 phase transition. For both NCM111 and NCM622, a clear redox peak is observed at 4.6 V, which could belong to an H2 → H3 phase transition or could also indicate an oxygen redox feature, in analogy to NCM811. The capacity retention of these NCMs cathode active materials is very stable up to the

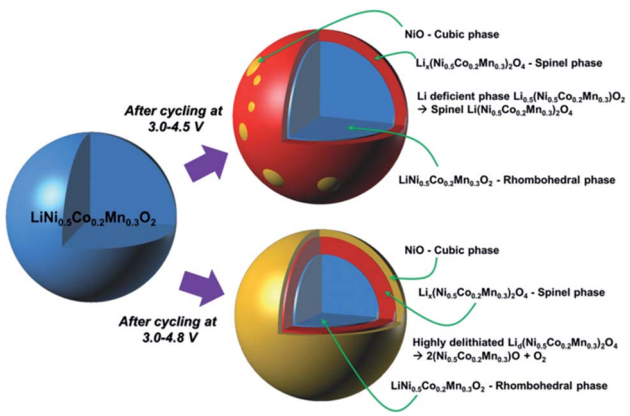

Fig. 4 Degradation mechanisms of $LiNi_{0.5}Co_{0.2}Mn_{0.3}O_2$ and phase transformation after cycle tests under high-voltage conditions.[44]

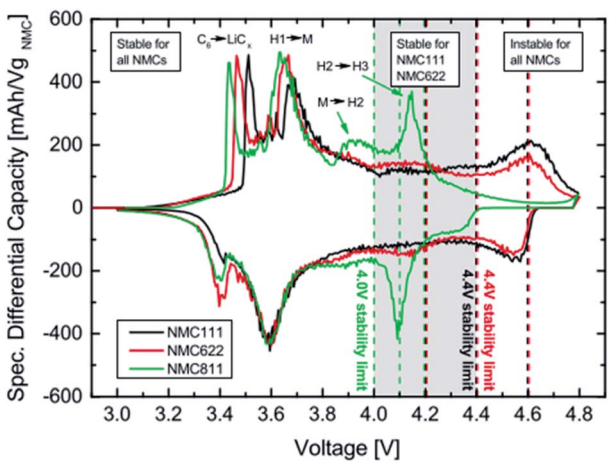

Fig. 5 Differential capacity *vs.* cell voltage of NCM-graphite cells recorded at a 0.1 C-rate (3rd cycle). The vertical dotted lines mark the upper cutoff voltages. The peaks are assigned to their corresponding phase transitions with H1, H2 and H3 representing the three hexagonal phases and M the monoclinic one. $C_6 \rightarrow LiC_x$ indicates the lithiation of graphite.[44]

onset of the H2 → H3 phase transition of NCM811 at above 4.0 V and up to the onset of the redox feature at above 4.4 V of NCM111 and NMC622. Therefore, stable cycling is only possible if the cutoff voltage is below the onset of the last peak in the plot. NCM811 cannot be cycled stably at above 4.0 V cutoff voltages due to the early onset of the H2 → H3 phase transition at above 4.0, whereas NCM111 and NCM622 cells show outstanding performance at potentials as high as 4.4 V. Multi-phase transitions of hexagonal to monoclinic (H1 → M), monoclinic to hexagonal (M → H2), and hexagonal to hexagonal (H2 → H3) during charging was also reported by Hyung-Joo Noh *et al.*[35]

3.2 Li^+/Ni^{2+} cation mixing

Cation mixing is the main reason for the capacity decline of the Ni-rich NCM cathode active materials.[29,55] As the Ni content in the NCM layered material increases the capacity will increase, which is the result of two-electron of Ni^{2+}/Ni^{4+} redox reaction but, increasing the Ni content results in a significant degree of mixing of Ni^{2+} and Li^+ cations due to the closeness of their ionic radius (Li^+ ~0.076 nm and Ni^{2+} ~0.069 nm).[48,49,55] In charged Ni-rich layered materials Ni^{3+}/Ni^{4+} are unstable and can easily be reduced to Ni^{2+}.[50,54] Because of their ionic radius similarity, the low energy barrier Ni^{2+} migrates from the sites in the transition metal layer to the available Li layer sites when the Li-ion is removed from Li layer sites during charging and promotes the Li^+/Ni^{2+} cation mixing. Thus, during discharge, Li^+ occupies the site of the available transition-metal layer. During migration, the Li^+ in the transition metal cannot be easily be extracted and the existence of Ni^{2+} in the Li layer blocks the diffusion of Li^+, resulting in both capacity loss and low rate performance.[48,51,52] In particular, a large proportion of Li^+/Ni^{2+} cation mixing can lead to increased strain and hinder the diffusion of lithium ions.[56] In addition to decreasing the diffusion rate of Li-ion, Li^+/Ni^{2+} cation mixing also reduces the amount of Li-ion participating in the charge/discharge reaction.

The structural instability can result from the disordered Li^+/Ni^{2+} cation mixing in NCM cathode materials. The Ni^{2+} in the Li position can cause the local structure collapse and accelerate the phase transition, hence, reducing the electrochemical performances of Ni-rich NCM materials.[57] Thus, the Li^+/Ni^{2+} cation mixing is related to the phase transformation, which may be performed by the kinetic mechanism and the thermodynamic driving force.[58] In this process, there are diffusion pathways, which can be divided into two separate processes: the atom-dominant and cell dominant process. Atom-dominant processes are related to Li and Ni atom exchange, in which Li-ions first migrate to a neighboring tetrahedral site, and the Ni-ion located below the tetrahedral Li site moves to the opposite tetrahedral site on the Li layer, forming a so-called Li–Ni dumbbell structure. In the cell-dominant process, Li and Ni ions migrate to a local minimum, forming a distorted five-fold square pyramid and finally, the square pyramids and the transition metal oxide octahedra slightly shuttle relative to each other in order to match the spinel lattice.[59] The Li^+/Ni^{2+} cation mixing can be present either during the materials synthesis process or during electrochemical cycling. The similarity of the ionic radius size of Ni^{2+} and Li^+ is the main reason for the formation of Li^+/Ni^{2+} cation mixing during the synthesis process. Li^+/Ni^{2+} exchange during synthesis is related to the layered to spinel transition, in which a Li–Ni dumbbell structure formation at high voltage. Even though such layered-to-spinel phase change is blocked by the cell-dominant pathway, Li–Ni cation mixing can be present as a side effect. Not only during synthesis process the Li^+/Ni^{2+} cation mixing can also occur during electrochemical cycle. In this case, Ni^{2+} ions first migrate to the tetrahedral positions of the Li layer (dumbbell) during charge and then move to the octahedral positions of the Li layer (Li^+/Ni^{2+} exchange) during discharge. The detailed mechanism of Li^+/Ni^{2+} exchange during electrochemical cycling is as follows: during charge, the enlarged interlayer distance facilitates the diffusion of Ni^{2+} to the Li layer, forming a dumbbell structure, especially at the lowest energy barrier for dumbbell formation. That is, the anti-site Ni^{2+} reduces the Li layer space, which decreases the Li^+ diffusion.[38] Ni^{2+} ions will then remain in the Li layer during the rest of the charging process owing to their high diffusion barrier in the Li layer. During discharge, Li-ions are inserted back into the Li layer and as well as into the now available Ni positions in the TM layer. The low energy required for Li^+/Ni^{2+} cation mixing at high Li concentration facilitates this process. After one charge/discharge cycle, only a certain amount of Li^+/Ni^{2+} cation mixing is present in the structure. However, as the *c* lattice parameter increases with Ni concentration, it can be inferred that NCM cathode materials with high Ni content suffer from more severe Li^+/Ni^{2+} cation mixing, which supports the large increase in Li^+/Ni^{2+} cation mixing after repeated charge/discharge cycles.[59] Li-ion in the transition metal layer has also a large activation energy barrier of Li-ion diffusion for the extraction of Li-ion from a transition metal, resulting in capacity fading of materials.[60,61] Gradually, the inverse Ni^{2+} in the Li layer can move to the surface of particles, leading to the depletion of Ni^{2+} in bulk. In other word, the anti-site Ni^{2+} can migrate to the material surface and destroys the stability of the structure, resulting in rate performance degradation and capacity fading.[38] Thus, the cationic mixing region on the particle surface is composed of NiO-like inactive phases, which worsen Li^+ diffusion and introduce thermal instability.[62]

The calcination temperature has also effects on the existence of Li^+/Ni^{2+} cation mixing. Hubert Ronduda *et al.*[63] have reported the effects of calcination temperature on $LiNi_{0.6}Mn_{0.2}Co_{0.2}O_2$ cathode materials and from PXRD results at a higher temperature, this material obtained its well-ordered structure. However, materials calcined at higher temperatures shows a higher Li^+/Ni^{2+} cation mixing, thus deteriorating their electrochemical properties.

According to studies by many researchers, the degree of Li^+/Ni^{2+} cation mixing can be identified from the XRD peak analysis.[61] In particular, the XRD peak of the Ni-rich NCM ratio of the intensities 003 and 004 peaks can determine the existence of Li^+/Ni^{2+} cation mixing. When the ratio of $I(003)/I(004)$ is less than 1.2 it shows the degree of cation mixing.[64] The process of this ratio reduction is as follows: when a cation disorder is generated, TM-ions occupy the lithium position, which leads to

a partial destructive interference of (003) plane's constructive interference at the Bragg angle of this peak by decreasing the intensity of (003) peak whereas, the intensity of (104) peak increases because TM-ions in Li-site also exist on the (104) plane.[43] In the XRD peak of Ni-rich NCM materials, the splitting degree of (006)/(012) and (018)/(110) peaks are important, which indicates whether the crystal materials are highly crystalline or not. The clear splitting of (006)/(102) and (018)/(110) peaks shows a high degree of layered structure crystallization.[65] As the Ni fraction in NCM increases, the peak splitting of (006)/(012) and (018)/(110) becomes unclear, indicating that the structure's disorder degree increased. If the ratio of I(003)/I(104) showing degree of cation mixing and the peak of (018)/(110) have been combining, the situation of serious cation mixing is occurred leading to some changes of the cell lattice parameters.[64] Controversially, researchers also reported that the Li^+/Ni^{2+} cation mixing has a positive effect on Ni-rich layered cathode materials, therefore the ordered mixing of Li^+ and Ni^{2+} can promote the structural stability of the cathode material.[66] Un-Hyuck Kim *et al.*[67] reported that the ordered intermixing of the Li and Ni ions structure in Ni-rich layered cathode materials. This ordered structure has the advantages of protecting the particle surface from structural degradation, reducing the voltage and capacity decay of cathode materials, and stabilizing the structure during cycling. Similarly, other studies have suggested that ordered Li^+/Ni^{2+} exchange may be beneficial to the electrochemical performance of batteries. These studies also show: (1) Li^+/Ni^{2+} exchange can mitigate the slab-distance contraction at high states of charge, thereby stabilizing the structure. (2) Although Li^+/Ni^{2+} exchange restricts the diffusion of Li-ions, it benefits the thermal stability of high-Ni NCM materials. Based on the above understandings, a balance between the negative and positive influences should be carefully considered so that an optimal degree of Li/Ni exchange for high-Ni NCM materials can be achieved in order to obtain the best electrochemical performance.[68]

3.3 Phase transformation

The crystal structures of the layered NCM cathode materials have a general formula L_xMO_2, which has a close-packed oxygen framework with the alkali L and the transition metal M cations filling alternating layers of interstitial sites.[21,28,39] It have an α-$NaFeO_2$ structure with an $R\bar{3}m$ space group,[7,40,69] which is a repeating O3 structure of oxygen–lithium–oxygen–transition metal–oxygen–lithium–oxygen–transition metal–oxygen along the rhombohedral as shown in (Fig. 6a),[43] where the L-ions occupy the site of 3a, M-ions occupy 3b, and O ions occupy 6c. The layers filled by M cations form an MO_2 slab consisting of edge-sharing MO_6 octahedral. The L cations, which can be shuttled between the MO_2 slabs, can occupy octahedral. During the charge, the type of O3 may change to the O1 and the structure of the cathode will transform from the $R\bar{3}m$ space group to disorder $Fd\bar{3}m$ space group then to the $Fm\bar{3}m$ space group in the end *via* the successional change of oxygen during cycling[70] (Fig. 6b). In addition, for lithium diffusion, the distance of slabs should become small to obtain a higher activation energy barrier.

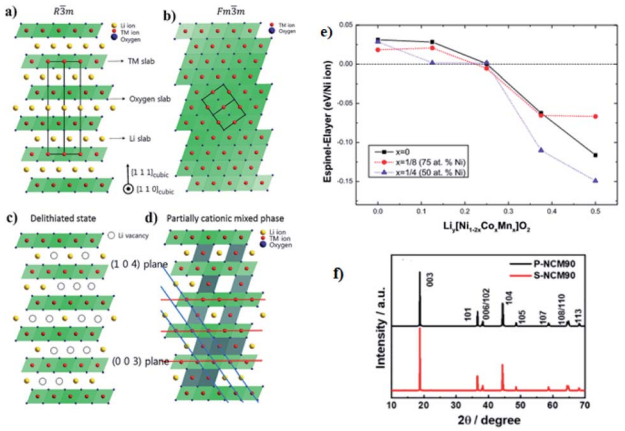

Fig. 6 [Illustration of the ordered and disordered phase in layered lithium metal oxides and their structural transformation. (a) Well-ordered $R\bar{3}m$ structure; (b) the cation disorder or cation mixing phase with $Fm\bar{3}m$ structure; (c) $R\bar{3}m$ structure with Li vacancies in highly charged state; (d) partially cation mixed phase with TM-ions in Li slab. Li atoms yellow, transition metals red, coordinated oxygen atoms dark blue].[43] (e) The relative stability between spinel and layered structure of $Li_yNi_{12x}Co_xMn_xO_2$ (x = 0, 1/8, and 1/4) as a function of Li concentration.[59] (f) XRD patterns of S-NCM90 and P-NCM90.[71]

During the process of removal of Li-ions from the host structure, NCM materials undergo the phase transition, which involves the cation disordering between TM site (octahedral 3a site) and Li site (octahedral 3b site) by forming $Fm\bar{3}m$ structure as shown in (Fig. 6b).[42,70,72,73] In a highly delithiated state, Ni-rich cathode material has an extremely unstable structure due to lithium vacancy (Fig. 6c), and this instability leads to TM-ion migration from the TM layer site to the Li layer site by forming spinel like phase (Fig. 6d).[43] In other words, during the removal of Li-ion, Ni-rich NCM materials undergo a series of phase transitions: the original layered structure (H1) transforms to the monoclinic phase (M), the second hexagonal phase (H2), and the third hexagonal phase (H3).[74] The difficulty to maintain all Ni-ions at the trivalent state and the ionic radius similarity of Ni^{2+} and Li^+ cations results in cation disorder phenomenon leading to an irreversible phase transition from a layered structure to a rock salt phase, indicating a greater Li-ion diffusion barrier and severe capacity fading.[75] This phase transition is also accompanied by the release of oxygen gas, which is an irreversible process and seriously deteriorates the performance of electrodes.[41] Specifically, the phase transformation of the layered to rock salt-like phase during repeated lithiation/delithiation causes structural degradation.[62] The chemical formula for the phase transition with the release of oxygen is as follows:[73]

$$3MO_2\ (R\bar{3}m) \rightarrow M_3O_4\ (Fd\bar{3}m) + 2[O] \quad (1)$$

$$M_3O_4\ (Fd\bar{3}m) \rightarrow 3MO\ (Fm\bar{3}m) + 2[O] \quad (2)$$

In Ni-rich NCM layered materials, phase transformation is usually observed at high voltages but not in bulk NCM.[76,77] The

layered to spinel phase transition in NCM is reversed after discharge.[78] We can easily investigate this reversible phase transition from the thermodynamics of layered-to-spinel phase transition in NCM cathode materials by comparing the total energy of the layered and spinel phases. Chaoping Liang *et al.*[59] have investigated this by comparing the total energy of the two-phase in $Li_yNi_{1-2x}Co_xMn_xO_2$ as observed in (Fig. 6e)[59] by using the first-principle calculations within the density functional theory with Hubbard parameter (DFT + U) framework. According to their study, when half of the Li ion ($y = 0.5$) is extracted from the host structure, the spinel phase is thermodynamically more favorable. However, the layered phase is thermodynamically more stable when $y < 0.25$ which indicates that the layered-to-spinel phase transition is reversible and the reversible layered-to-spinel transition point would be at $y = 0.25$. The experimental observation has also supported the fact that the layered-to-spinel phase transition can be reversible during electrochemical cycles.[79] Therefore, the layered-to-spinel phase transformations in Ni-rich NCM are often not severe to the electrochemical performance. The spinel phase has much higher voltage than that of its layered phase, which is used to prevent the dissolution of TM ions in the highly delithiated state, and it can be used as a coating material for NCM.[80]

The phase transition from layered-to-rock salt phase is very serious for the electrochemical performance of Ni-rich cathode materials. Accordingly, after discharge, the phase change on the surface of Ni-rich NCM particles always needs to be reversed.[59] However, the rocksalt phase changes occurring on the surface particles are always not reversible and it seriously affects the electrochemical performance of the materials.[81] This phase will be accumulated at the electrode/electrolyte interface, forming a NiO surface film. Thus, the resulting NiO surface-film impedes the transport of Li^+, and Li^+ is irreversibly consumed in its formation.[48] The reduced Ni^{2+} greatly accelerates the formation of an irreversible phase transition from the layered to NiO rocksalt phase.[82] At high charge voltage, the deep lithium removal results in enough lithium vacancies and it leads to accelerates this phase transition process, exhibits structural degradation, and causes decreasing of voltage continuously.[83] Phase transition causes stacking defects, which increase the diffusion kinetic energy barrier of Li-ion and cause the difference of the diffusion rates of Li-ion in various directions as they pass *via* the stacking defects.[84] The existence of a disordered rock-salt-like structure not only hinders the intercalation of Li^+ during discharging for the occupation of TM ions at the Li^+ site, leading to severe irreversible capacity loss, but also increases the energy barrier for Li^+ diffusion due to its smaller distance between slabs, resulting in a low Li^+ diffusion rate.[85] The formation of the phase transition in Ni-rich NCM materials may also depend on the cycling rate in addition to involves the Li^+/Ni^{2+} cation mixing. Lianfeng Zou *et al.*[86] have demonstrated that varying the cycling rate changes phase transition products in Ni-rich $LiNi_{0.76}Co_{0.10}Mn_{0.14}O_2$ by using scanning transmission electron microscopy (STEM) and atomic simulation. Fig. 7 shows their pictorial representation of the structure evolution of Ni-rich $LiNi_{0.76}Co_{0.10}Mn_{0.14}O_2$ materials at low and high rates. Varying with the cycling rate, the as-synthesized product layered

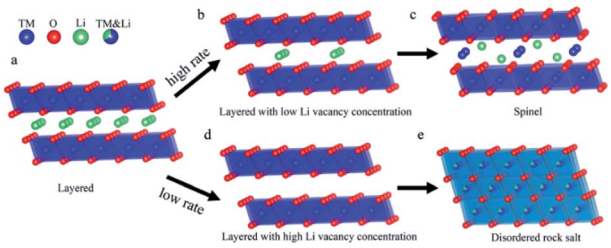

Fig. 7 Pictorial illustration of the phase transition occurring at distinct cycling rates. (a) The starting layered structure. (b) The delithiated state under the high cycling rate, creating limited amount of Li vacancies. (c) The structure evolution toward the spinel structure. (d) The delithiated state under the low cycling rate, generating significant amount of Li vacancies. (e) Formation of disordered rock salt structure.[86]

structure undergoes a variety of depths of discharge upon cycling. The $LiNi_{0.76}Co_{0.10}Mn_{0.14}O_2$ cathode that cycled at a high rate *i.e.* 2C is generating vacancies, yet accompanied by a large fraction of Li^+ remaining in the layered structure which results limited number of Ni^{2+} to migrate into the lithium position causing spinel phase (Fig. 7d). In contrast, $LiNi_{0.76}Co_{0.10}Mn_{0.14}O_2$ materials with a slow discharge rate, *i.e.*, below 1C, offer the opportunity for adequate draining of Li-ions. The low rate results the disordered rocksalt phase changes (Fig. 7e).

The surface degradation of the layered structure of the cubic NiO rocksalt is also accompanied by oxygen evolution and heating. Bak *et al.*[87] have investigated structural changes and gas evolution during the thermal decomposition of charged Ni-rich cathode materials by combining *in situ* time-resolved X-ray diffraction (TR-XRD) and mass spectroscopy (MS). For structural changes, they reported that the phase transition from the rhombohedral (space group $R\bar{3}m$) to disordered spinel starts at 194 °C. This disordered spinel phase gradually transformed to the rocksalt phase as the temperature increased from 275 °C to 500 °C. Due to the irreversible structural degradation of large surfaces, materials are at risk of thermal runaway and loss of active materials.[88] From the XRD patterns results, many researchers have proved that the Ni-rich cathode materials can be identified as either it is layered or not. Recently, Hoon-Hee Ryu *et al.*[71] have studied that the powder XRD patterns of both single-crystalline Ni-rich NCM with Ni content 90% (S-NCM90) and polycrystalline NCM90 (P-NCM90) and they observed that as shown in Fig. 6f, which both have a hexagonal α-$NaFeO_2$-type structure belonging to the $R\bar{3}m$ space group and without impurities detection.

According to some research studies, the orderly accumulated rocksalt on the particle surface can improve the cyclic and thermal stability of materials. Yuefeng Su *et al.*[89] have reported an improvement of the cycling stability of Ni-rich $LiNi_{0.8}Co_{0.1}Mn_{0.1}O_2$ cathode materials by fabricating the surface rock salt phase. They have shown that the fabrication of Ni-rich materials with a surface rock salt phase results in better structural stability and electrochemical performances, in which the rearrangement of the irreversible structure leads to the passivation of the rocksalt phase on the surface and leads to loss of electronic conductivity and structural instability of the materials.[72]

3.4 Microcrack generation

The structural degradation of the NCM particles and the electrode due to volumetric changes of the rhombohedral structure upon repeated delithiation/lithiation of the NCM crystallites is one of the proposed failure mechanisms of Ni-rich NCM materials.[90] Thus, the volumetric changes of the rhombohedral structure causes the microcracks in Ni-rich cathode material that categorized as mechanical failure and largely cause the rapid capacity fading of Ni-rich layered cathodes in the deeply charged state. Microcracks increase the exposed internal surface by creating crack faces and serve as channels through which the electrolyte can penetrate the particle interior.[91] Subsequent degradation of the exposed internal surfaces through parasitic electrolyte attack accelerates the accumulation of NiO-like insulating layers at the cathode/electrolyte interfaces that inhibit lithium diffusion. The NiO-like insulating layers accumulated at the cathode/electrolyte interface forms the cathode electrolyte interface (CEI), which is analogous with the solid electrolyte interface (SEI) formed at the anode/electrolyte interface.[91,92] As a result, the first formed CEI will be disrupted and then be rebuilt new one by consuming active lithium from the electrolyte.[29,44]

Furthermore, penetration of electrolytes through cracks not only accelerates the formation of the CEI layers, but also causes voltage decay.[93] The stable CEI helps for the performance of cathode, but the continuous formation on the newly formed surface of active materials due to crack formation will cause the capacity decline.[94] From most of the previous studies for investigation of particle cracking, the electrodes should have to be harvested from the cycled cells and prepared and analyzed by Kr-BET, FIB-SEM, or TEM, which are difficult and furthermore require a large number of repeat analyses to be statistically significant. Stefan Oswald *et al.*[90] have introduced a novel method based on electrochemical impedance spectroscopy (EIS) in blocking conditions to quantify the increase in the active material's surface area upon cycling, utilizing the correlation between the surface area of the electrode and the electrochemical double-layer capacitance that is validated experimentally by comparing the capacitance and BET surface area increase of NCM electrodes upon mechanical compression. To quantify the cracking of the particles after 200 charge/discharge cycles, they perform *in situ* EIS measurements utilizing a micro-reference electrode and monitor the cathode's impedance response and found surface area increment of up to ~261%.

Microcracks in cathode particles originate from the local strain build-up caused by their highly anisotropic contraction and expansion during Li^+ intercalation/de-intercalation.[95] Thus, Li^+ intercalation/de-intercalation behavior during charging and discharging of Ni-rich cathode materials can cause significant volume changes, resulting in micro-strain and crack formation of particles, which further leading to the internal and interstitial splitting of crystals.[34,76] Lead de Biasi *et al.*[36] have reported the increasing of the volume change of the NCM unit cell with the nickel content by using operand X-ray diffraction combined with detailed Rietveld analysis. They correlated energy density with X-ray diffraction results and they found that irrespective of the Ni contents, all NCM materials are subjected to structural changes during operation. The change of the unit cell is due to the contraction and expansion of both *a*-axis and the *c*-axis lattice parameters, which results in changes in the *c*/*a* ratio upon repeated charge/discharge that are accompanied by severe stress and strain. This leads them to the assumption that increasing the Ni content results in major challenges in terms of mechanical strain and structural degradation.

Simon Schweidler *et al.*[96] investigated mechanical degradation and fatigue of Ni-rich NCM cathode material (NCM851005) in graphite-based full cells by using galvanostatic charge/discharge tests, electrochemical impedance, XRD and electron microscopy. They found that microcracks formation can be increased by increasing the number of cycles. Fig. 8a–f shows that the SEM examines morphological changes of the primary and secondary particle levels. Particles morphology after 100 and 500 cycles are shown in (Fig. 8c–f) and more fractured secondary particles are observed, some of them having a flattened structure at the top surface.[86,96] These particles suffered from cracking due to electrochemical cycling. Finally they suggested that the capacity fading is associated to some with the mechanical degradation of the cathode material. Moreover, anisotropic volume changes during delithiation/lithiation impart stress into the material, leading to particle fracture.

Hoon-Hee Ryu *et al.*,[97] have also reported, the capacity fading of Ni-rich NCM cathodes, especially above $x = 0.8$, where x is the Ni content in the NCM composition, largely due to the anisotropic volume change, which is caused by the phase transition. Repeated, nonuniform contraction and expansion during cycling generated internal microcracks that propagated to the particle surface, opening channels for electrolyte infiltration into the particle interior. General speaking, when the content of Ni in the NCM composition increases, this phenomenon becomes more evident.[98]

The general consequences of particle cracking include: loss of electrical contact NCM active particles, conductive additives and current collectors; increased the growth rate of CEI layer; and electrode pulverizations. All the above phenomena suffer a decrease in electrochemical performance and hinder the widely commercialization of Ni-rich materials.[99] Thus, currently

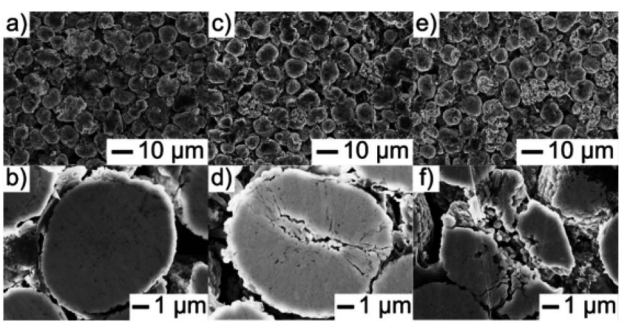

Fig. 8 Top view and cross-sectional SEM images of the NCM851005 cathode in discharged state (a and b) before cycling and (c and d) after 100 and (e and f) 500 cycles at 1C and 45 °C.[96]

the cracking issue has been identified as a major degradation mechanism.

3.5 Electrolyte decomposition

One of the most important issues in Ni-rich cathode materials is the surface damage caused by the parasitic reaction between the cathode material and the organic electrolytes.[91] The cathode surface damage causes the capacity decay for full battery cells, which accelerates the electrolyte decomposition. The electrolyte decomposition is more severe the degradation of the cathode materials surface structure, increasing cathode surface impedance. That is, the degradation of the cathode material surface caused by electrolyte erosion is the main reason for the increase in charge resistance during cycling.[79] High temperature and high state of charge are the root cause for the decomposition of electrolyte. The battery capacity will gradually decline and the material's structure will change as these side reactions occur, and it will become more severe at high operating voltage.[19] At the high state of charge (>4.5 V), Ni^{2+} will be oxidized to highly reactive Ni^{4+} form, which reacts with the organic electrolyte, releasing O_2 and forming a NiO-like phase.[100] Thus, the poor cycling performance is partial because the increased amount of unstable Ni^{4+} formed during the charging process strongly reacts with the electrolyte and leaves more side products.[101] This causes depletes the electrolytes and propagates the undesirable thick cathode electrolyte interface (CEI) layer at the interface, thus increasing the impedance of NCM materials.[73,100] This is because the labile Ni^{4+} species are prostrate to transform to more stable chemical states (Ni^{3+}or Ni^{2+}) by reduction, the electrolyte can be promptly decomposed at the electrolyte/electrode interface, thereby affording electrons to Ni^{4+}.[102] The unstable Ni^{4+} during highly delithiated can cause surface instability. For example, if $LiPF_6$ is used as an electrolyte, it can be decomposed into LiF and PF_5 under the high catalytic activity of Ni^{4+}. From the results of the decomposition, LiF play great role in the formation CEI layer and increases the cathode impedance, while PF_5 reacts with H_2O to form acid HF.[88,89] Furthermore, the electrolyte $LiPF_6$ salt is unstable in the presence of H_2O molecules and, at high temperature or high operation voltage, is decomposed by the following eqn (3) and the produced PF_5 react with water by forming the very dangerous acid that can attack the active materials surfaces eqn (4):[69,96]

$$LiPF_6 \rightarrow LiF + PF_5 \quad (3)$$

$$PF_5 + H_2O \rightarrow POF_3 + 2HF \quad (4)$$

Furthermore, due to the existence of Ni^{4+}, the surface structure of the material is unstable, and it is easy to be eroded by hydrofluoric acid in the electrolyte during high voltage charging, which makes the capacity of LIBs decay faster.[103] Hence, continuous reactions between highly delithiated cathode materials and electrolytes result in structural instability, increasing interfacial resistance, and rapid capacity fading.[39]

As discussed in Section 3.4 CEI can be formed due to the crack formation of the active materials, in which once crack is formed, new CEI will be formed on each newly formed surface of active materials. Additionally, as discussed in this section, CEI can be formed on the Ni-rich cathode materials by the oxidation of electrolytes.[50] Ikuma Takahashi *et al.*[94] have used hard X-ray photoelectron spectroscopy (HAXPES), soft X-ray absorption spectroscopy (S-XAS), and density functional theory (DFT) analyses, to investigate the formation of CEI on Ni-rich cathode surfaces and electrolyte oxidation mechanisms. For the formation of CEI, they have proposed two electrolyte oxidations: (i) oxidation electrolyte solvent which forms Li_2CO_3 and alkyl carbonates on Ni-rich NCM and when electrolytes proceed continuously during charge/discharge cycles the amount of Li_2CO_3 and alkyl carbonate increases; (ii) oxidation of electrolyte salt, which produces $Li_xPO_yF_z$ and its amount increases during the continuous charge/discharge cycles. Then the oxidizing of the electrolyte solvent and salt continues by Ni-rich cathode, and forms continuously the CEI that consists of Li_2CO_3, alkyl carbonate, and $Li_xPO_yF_z$ during the charge/discharge cycles. From their S-XAS and DFT studies, for the Ni-rich cathode at the delithiated state, they have indicated that the energy of the antibonding hybrid orbital of the TM 3d–O 2p corresponds to the LUMO energy level of the hole for the Ni-rich cathode at the charged state. Thus, the LUMO energy level decreases from the discharged to the charged state and lies close to the HOMO energy level of the electrolyte, and becomes very close to Fermi level as shown in (Fig. 9). They have also observed a high increase in hole concentration. The closeness of the LUMO energy level of a Ni-rich cathode to the HOMO energy level of the electrolyte and the high hole concentration of the Ni-rich cathode produce oxidation of the electrolyte, forming a thick CEI for the Ni-rich cathode.

3.6 Transition metal dissolution

The transition metals (TMs) dissolution also causes the capacity degradation of Ni-rich NCM cathode materials. The root cause of transition metal dissolutions are the high state of charge and high temperature.[104] Transition metal dissolution is ascribed to a combined effect of the cation mixing and oxygen evolution reaction, in which the cation mixing accompanies the entire life of the battery while the oxygen evolution occurs mainly in the H3 phase. On the one hand, the cation mixing and the oxygen evolution reaction result in the formation of low-valence

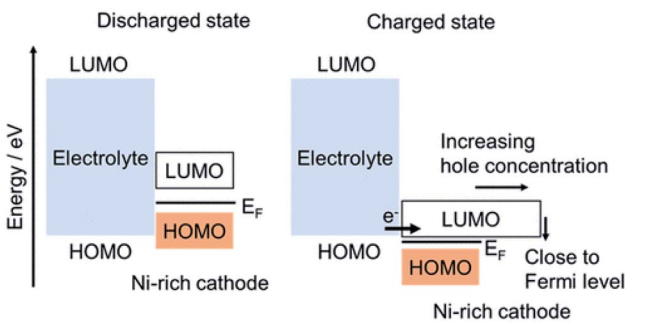

Fig. 9 The HOMO and LUMO of electrolyte and Ni-rich cathode forming oxidation of electrolyte and CEI.[94]

transition metal oxide (MO) by the loss of oxygen.[73] The gas evolution of CO_2 and CO is accompanied by the formation of H_2O. As displayed in eqn (5), the formed H_2O hydrolyzes the $LiPF_6$ resulting HF (eqn (4)) and then HF reacts with low valence transition metal oxide (MO) which is occurred by the loss of oxygen, resulting in the collapse of the surface structure and the rapid decay of the reversible capacity:[27]

$$HF + MO \rightarrow H_2O + MF_2 \quad (5)$$

In other word, these acid species react with NCM cathode active materials, resulting in transition metal dissolution ions. These dissolute TMs may include $Ni^{2+}/Ni^{3+}/Ni^{4+}$, Mn^{3+}/Mn^{4+} and/or Co^{3+}/Co^{4+} and they react with electrolyte to form MF_2, resulting deposition of MF_2 onto the NCM surfaces to form thick layer.[50]

Electrolyte decomposition also causes the formation of fluoride (F^-) in the cell, which seriously accelerates the dissolution of transition metal components from the Ni-rich NCM cathode materials *via* chemical reactions and these reactions further accelerated at elevated temperature.[105] The volume change of Ni-rich cathode materials during the charge/discharge cycles results in lattice parameter distance alter and produces microcracks generation inside or between the primary particles.[106] The produced microcracks increase the contact area between the particle interior and the electrolyte, which ultimately accelerates the degradation of the cathode material and results in TMs dissolution.[107] The dissolution of transition metals is deposited on the surface electrodes especially on the surface of the anode which hinders the diffusion of Li-ions, resulting in a decrease in the electrochemical performance of the battery.[108] When the migration and deposition of dissolved metal ions on anode increases, Li-ion intercalation/de-intercalation between electrolyte and electrode interface disrupts, hence increasing the impedance and it can form a growth of dendrites. The deposition of TMs on the anode surface can be confirmed by X-ray absorption, X-ray fluorescence, magnetic resonance spectroscopy and electron probe microanalysis (EPMA) analyses.[107] Dong-Su Ko *et al.*[107] determined the dissolution mechanism and micro-structure origin of TMs from Ni-rich $LiNi_{0.87}Co_{0.9}Mn_{0.4}O_2$ cathode material and its migration into the electrolyte and deposition at the anode. Their results verified that TM dissolution preferentially occurred for particles with high surface area/volume ratios. Furthermore, they recommended that high-resolution chemical composition analysis, providing a powerful technique for investigating the degradation phenomena in lithium-ion batteries.

3.7 Residual lithium compounds

The residual lithium compounds are present as in a manner that is impossible to avoid in a Ni-rich layered oxide and their amount increases with Ni content, which will aggravate the deterioration of the material's electrochemical performance.[103] This lithium residual is present initially in the form of Li_2O and gradually changes to Li_2CO_3 and LiOH by reacting with H_2O and CO_2 in the air.[73] Thus, the Ni-rich materials have shown fast moisture and CO_2 uptakes in air, originating from the active oxygen species upon the reduction of Ni^{3+} to Ni^{2+} and synthetic Li impurities of Li_2O/LiOH on the surface.[36,104] Such absorption would also result in high pH of Ni-rich NCM particles that cause the gelation of cathode slurry.[75] In short, the lithium residual originates from two sources. The first one is due to an excess amount of lithium precursors introduced in the synthesis, which are required to achieve the ordered layered structure that could provide better capacity.[109] In this case, lithium will be volatile in the process of high-temperature sintering, the addition of excessive Li precursors can effectively inhibit the Li/TMs cation mixing and this cation mixing could slightly increase to compensate for the loss during the sintering process.[110] As a result, extra Li-ions will live on the surface of cathode materials in form of Li_2O and reaction of lithium residues with H_2O and CO_2 in air, meaning that the Li_2O on the outer surface of the active materials converted to Li_2CO_3, $LiHCO_3$, and LiOH layers after exposed to air.[57,64,97]

The lithium residual reaction with CO_2 and H_2O in formula (6)–(8):[111]

$$Li_2O + CO_2 \rightarrow Li_2CO_3 \quad (6)$$

$$Li_2O + H_2O \rightarrow 2LiOH \quad (7)$$

$$2LiOH + CO_2 \rightarrow Li_2CO_3 + H_2O \quad (8)$$

The second is from the slow spontaneous reduction of Ni^{3+} to Ni^{2+} and the corresponding lattice oxygen O^{2-} will be oxidized to O^- and then the active O^{2-} will be generated on the surface of cathode materials. The combination of active O^{2-} and Li-ions in the materials will form Li_2O which reacts with H_2O and CO_2 in the air to form residual lithium compounds on the surface of Ni-rich NCM cathode materials. The Li_2CO_3/LiOH impurities on the surface of the cathode materials would further react with HF generated from the decomposition of $LiPF_6$ in the electrolyte (eqn (9)), resulting in gas evolution and consequent safety problems.[112]

Chemical and/or physical adsorption of residual lithium compounds such as Li_2O/LiOH on the surface of the materials cause the rapid moisture absorption of Ni-rich cathode materials. Hence, through the LiOH and Li_2CO_3 titrations, it is confirmed that the Li_2O on the active materials induces more formation of LiOH and, in particular, Li_2CO_3 on the surface of active materials (Fig. 10a).[111] The Li_2CO_3 promotes the gas evolution and increases the moisture of the Ni-rich cathodes and the LiOH increases the powder pH value causing of slurry gelation during electrode fabrication.[113] Furthermore, these undesirable LiOH and Li_2CO_3 species are the main component of residual lithium compound and impede the diffusion of Li^+ due to their insulating properties, and deteriorate the electrochemical cycle performance of the Ni-rich cathode materials.[114] Sung Wook Doo *et al.*[115] have performed pH titration to measure changes in the amount of residual lithium compounds before and after the storage. As shown in (Fig. 10b), the total amount of residual lithium compounds substantially increased after storage in humid CO_2, while negligible increases in residual

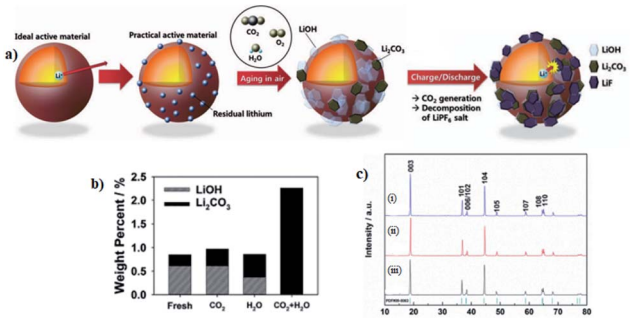

Fig. 10 (a) Surface change of $LiNi_{0.7}Mn_{0.3}O_2$ materials after exposure in air and effect of the residual lithium on the surface of $LiNi_{0.7}Mn_{0.3}O_2$.[111] (b) The amounts of residual lithium compounds on the $LiNi_{0.8}Co_{0.1}Mn_{0.1}O_2$ surface measured from titration.[115] (c) XRD patterns of $LiNi_{0.8}Co_{0.1}Mn_{0.1}O_2$ with Li excesses (i) 20%, (ii) 10%, and (iii) 0%, where some of the minor peaks are residual lithium compound impurities.[65]

lithium compounds were measured after storage in dry CO_2 and in humid Ar.

From eqn (4) the formed HF can react with the residual lithium compound to form CO_2 and the formed CO_2 react with Li-ions to form CO as illustrated in eqn (9) and (10) respectively:[116]

$$Li_2CO_3 + 2HF \rightarrow 2LiF + H_2O + CO_2 \quad (9)$$

$$2CO_2 + 2Li^+ + 2e^- \rightarrow Li_2CO_3 + CO \quad (10)$$

Side reactions at the interface of electrode/electrolyte can also be caused by the residual lithium, accelerating the electrolyte decomposition and forming thick cathode electrolyte interface (CEI), which can affect Li-ions diffusion pathways:[57,96]

$$LiPF_6 + 2LiOH \rightarrow 3LiF + POF_3 + H_2O \quad (11)$$

$$LiPF_6 + H_2O \rightarrow LiF + 2HF + POF_3 \quad (12)$$

$$POF_3 + nLi^+ + ne^- \rightarrow LiF + Li_xPO_yF_z \text{ or} \quad (13)$$

$$2POF_3 + 3Li_2O \rightarrow 6LiF\downarrow + P_2O_5\downarrow \text{ (or } Li_xPO_yF_z) \quad (14)$$

HF produced by the reaction of lithium residue with LPF_6 in electrolyte results in high pH of Ni-rich particles, which results in the gelation of cathode slurry.[117] The reduction of Ni^{3+} to Ni^{2+} on the surface of Ni-rich layered materials occurs spontaneously in the air. The residual lithium on the surface of the Ni-rich NCM absorbs carbon dioxide and water from the ambient air as mentioned before.

The presence of residual lithium compounds can be also detected by powder X-ray diffraction (XRD) measurement, Fourier transformed infrared spectrum (FT-IR) and X-ray photoelectron spectroscopy (XPS) spectra analysis, titration method, and Transmission Electron Microscope (TEM) detecting technique.[110] For instant, Feng Wu *et al.*[65] have reported the Li excess $LiNi_{0.8}Co_{0.1}Mn_{0.1}O_2$ that was produced by sintering the $Ni_{0.8}Co_{0.1}Mn_{0.1}(OH)_2$ precursor with different amounts of a lithium source, and from XRD result they have identified that some minor peaks (Fig. 10c), which are assigned to LiOH and Li_2CO_3 emerged because some amount of LiOH remains and reacts with CO_2 in the air to form Li_2CO_3 during the synthetic process.

Lithium residues can also react with slurry components during mixing and may become gels due to the polymerization of *N*-methyl-2-pyrrolidone (NMP), which makes it difficult to coat the electrodes on the aluminum foil surface and complicates the preparation of the electrodes.[118,133] The washing process is usually used to remove lithium impurities in NCM to avoid lithium residue.[118] Although this easy method is attractive in practical applications, it leads to loss of oxygen in the lattice during the immersion of Ni-rich materials, resulting in a NiO defect, which leads to a decrease in the specific capacity of the material after washing.[119] In general, two inactive phases can be formed on the surface-active cathode materials in the presence of lithium residue. These are rock-salt NiO phase and Li_2CO_3/LiOH layer, which are electrochemically inactive for Li-ion intercalation/deintercalation processes and lead to high cathode resistance and severe capacity degradation.[124]

3.8 Oxygen release and evolution of CO_2 and CO

The structural instability of layered oxide cathode materials can lead to the release of oxygen in the form of O_2 or forms reactive peroxide species.[50] The mechanism of layered oxide cathode material's oxygen release may be related to external local temperature rises, which initiates the undesired reactions that lead to the thermal runaway.[120] At the risen temperature, the SEI on the anode can be breakdown and further rises up the temperature.[121] The breakdown SEI triggers the side reactions between anode and alkyl carbonate electrolyte by forming combustible gas ethane and methane. Then, the polymer separator between the anode and cathode will melt down causing a short circuit between the two electrodes.[122] Ultimately, the layered oxide materials decompose and release a large amount of oxygen.[120]

On the other hand, at a highly delithiated state, Ni-rich cathode materials become unstable and tend to be more stable when oxygen is released,[87] which may decompose through phase transitions (MO_2 (layered) → M_3O_4 (spinel) → MO (rock-salt)). The resulting decomposition of the charged cathode materials can result in the release of oxygen-containing species, which are highly reactive.[40] Thus, in layered oxide Ni-rich NCM materials the highly oxidized state of Ni^{4+} in the highly delithiated state, during electrochemical reactions tend to form permanent surface reconstruction layers such as spinel and rock-salt phases, which subsequently cause oxygen release. The released O_2 can react with a flammable organic electrolyte, leading to massive heat and severe safety hazards, such as flames and explosions.[6,20,65] Oxygen release in Ni-rich cathode materials can be related to phase transition and this phase transition mainly depends on the Ni content related to temperature, that is as Ni content in NCM start to increases, the phase transitions occurred at low temperatures.[123] If there is no phase transition, there is no oxygen release, which results in

good thermal stability. For low Ni contents, there is no much oxygen release. The existence of nanopores also strongly affects the degradation of Ni-rich NCM cathode materials as the pore surfaces apparently increase oxygen loss and formation of rock-salt regions.[124]

The cathodes oxygen release can be investigated by thermal analysis, time-resolved X-ray diffraction (TR-XRD), Raman spectroscopy, *in situ* differential electrochemical mass spectroscopy (DEMS), X-ray absorption spectroscopy (XAS), *in situ* transmission electron microscopy (TEM), and computational modeling.[135] Various study revealed that the O_2 evolution is a complex mechanism that is influenced by many parameters such as state of charge (SOC), morphology and size of the particles, chemical composition, and atomic arrangements of the cathodes.[120] For instance, Seong-Min Bak *et al.*[97] have been used the combination of *in situ* time-resolved X-ray diffraction (TR-XRD) and mass spectroscopy (MS) to study the structural change and gas evolution of Ni-rich cathode material. From this combination, they simultaneously observed the structural changes and gas species that are evolved during the thermal decomposition of charged cathode materials. In addition, Chengyu Mao *et al.*[125] have been used gas chromatography-mass spectrometry (GC-MS) and Fourier transform infrared spectroscopy (FTIR) to identify gas species evolved from the full cell of NCM811 cathode and a graphite anode.

The appearance of oxygen vacancies on the surface of cathode materials is a direct consequence of oxygen evolution.[126] Similarly, Kyoungmin Min *et al.*[127] have been used first-principles calculations to identify the effects of oxygen vacancy. Thus, when oxygen vacancies are present, Ni can migrate to the Li site during delithiation. For the highly delithiated Ni-rich cathodes, the increase in temperature will induce a series of phase changes and side reactions. As a result, reactive oxygen-containing species are produced, which, together with Ni^{4+}, oxidizes the electrolyte to release gaseous side-products, such as CO_2 and CO.[44] The evolution of both CO and CO_2 in Ni-rich cathode materials can be occurred by two mechanisms:[128] (i) electrochemical oxidation of electrolyte, which is either proportional to the sum of the total surface areas of the cathode active material (CAM) and the conductive carbon if it is a non-catalytic process or to only the CAM surface area if catalyzed by transition metals at the layered oxide surface, and (ii) chemical oxidation of electrolyte caused by the release of reactive oxygen from the Ni-rich NCM surface, in which case the oxidation rate would again only depend on the CAM surface area.[123,129] When these released reactive [O] also reacts with ethylene carbonate (EC) it forms CO_2 and CO and H_2O as following reaction:[92,127]

$$EC + [O] \rightarrow CO_2(g) + CO(g) + H_2O \quad (15)$$

In Ni-rich NCM materials the oxygen releases that consequence the evolution of both CO_2 and CO by reaction with alkyl carbonate electrolyte also depends on temperature. Roland Jung *et al.*[130] have reported that the temperature dependence of oxygen release and evolution of CO_2 and CO of NCM622 by using OEMS, hence the amount of CO_2 and CO evolution occurred simultaneously with O_2 release increase with temperature. Toru Hatsukade *et al.*[131] studied the contributions of different mechanisms to the generation of CO_2 for layered NCM cathode materials by using the combinations of isotope labeling, electrolyte substitution, and *in situ* gas analysis. They found that Li_2CO_3 decomposition contributes to CO_2 evolution and significant during the first cycle but evolution rapidly decreased with subsequent cycles at high potentials. They also reported the major contribution of electrolyte decomposition for CO_2 evolution.

Oxygen release in Ni-rich cathode materials can also be related to state-of-charge (SOC). Daniel Pritzl *et al.*[132] have investigated the effect of washing/drying on the gas evolution of a Ni-rich NCM materials in the first charge to high SOC by performing on-line electrochemical mass spectrometry (OEMS) on electrodes with the pristine and the washed NCM-851005. The OEMS in terms of gassing revealed that the release of O_2 and CO_2 above 80% SOC decreases substantially as the drying temperature of the washed NCM-851005 increased from 25 °C to 300 °C, along with the cathode impedance. In NCMs, the oxygen evolution stops after some cycles, whereas the formation of CO and CO_2 from cycle to cycle decreases at a much slower rate. Generally, the evolution of gases raises a serious safety concern on Ni-rich NCM cathode materials.[101]

3.9 Thermal instability

In several LIBs powered systems ranging from laptops and cell phones to e-cigarettes, headphones, electric vehicles, and even airplanes, thermal runaway events have been observed and have caused serious injuries to the consumers.[75,103,108] A series of self-progressive exothermic events triggered by external factors such as ambient temperature rise or mechanical abuse, or caused by internal factors such as a short circuit, overcharge or applied high current rates results in the thermal runaway.[109,110,112,113] Thermal runaway is the main cause of safety accidents such as fire and explosion of LIBs.[110,112] The occurrence and sequence of these chains of events can vary based on the materials design and the specific conditions that trigger the thermal runaway reaction.[103,110] Studies on the thermal stability of Ni-based cathode materials by thermogravimetric analysis (TGA), differential scanning calorimetry (DSC), differential thermal analysis (DTA), thermogravimetric analysis coupled with mass spectrometry (TGA-MS), *in situ* high-temperature X-ray diffraction (XRD), and accelerating rate calorimetry (ARC) show that the thermal decomposition reaction in charged cathodes starts at lower onset temperatures with increasing Ni content in the cathode materials, which indicates that a high Ni content worsens the thermal stability of the cathode materials.[113,114]

In their charged states, the layered oxide cathode materials are metastable under ambient air, but at elevated temperatures, they begin to decompose and release O_2 due to the high effective oxygen partial pressure.[133] Specifically, at highly delithiated states in the Ni-rich cathode materials, the reduction of Ni^{4+} to Ni^{2+} during heating releases O_2 and the released O_2 reacts with the flammable electrolytes causing severe thermal runaway and lead to catastrophic failure of the LIBs. In Ni-rich cathode materials, O_2-release-related safety concern is the main

drawback, despite its obvious advantage in high capacity. Thus, the safety hazards in Ni-rich cathode materials are ascribed to thermodynamic instability of H3 phase, which increases with state of charge and temperature.[73] In H3 phase, the delithiated Ni-rich cathodes materials are very thermodynamically unstable, which results in either chemically oxidize electrolyte solvents or spontaneously release O_2. These cause safety hazards during charging and storage due to hot conditions. The oxidized electrolyte solvent generates heat and gaseous products. The processes of safety hazard include the O_2 evolution reaction intermediate and the dissolved O_2 passes through the separator and reach the anode. And then chemically react with the lithiated anode. This is a reaction far more energetic than the reaction with electrolyte solvents, which results in the thermal runaway of LIBs initiating without needing of internal electric shorting.[73]

Furthermore, in the presence of temperature effects, as Ni content in NCM starts to increases, the phase transitions occurred at low temperatures.[123] Fig. 11 shows the phase transitions and cation migration paths of transition metal in the charged NCM cathode materials during thermal decomposition. In the initial layered structure (Fig. 11a), the TM cations occupy octahedral positions (TM_{oct} layer) and the Li^+ occupy the alternate layers of octahedral sites (Li_{oct} layer). For the first phase transition from the layered to the disordered spinel, some of TM cations need to migrate from their original sites (labeled "A" in Fig. 11b) to the octahedral positions in the Li layer (labeled "B" in Fig. 11b). This migration will take place through the nearest tetrahedral position *via* the face-shared neighboring octahedra. Because of its lower energy barrier, it is well-known that this tetrahedral pathway of O_h (the octahedral site in TM layer)–T_d (tetrahedral site)–O_h (octahedral site in Li layer) is energetically favorable. This must be accompanied by the movement of Li^+ from their original positions to the adjacent tetrahedral positions to complete this first phase transition to the $LiMn_2O_4$-type spinel structure, as shown in (Fig. 11c). Such a structural change is accompanied by the reduction of TM cations and O_2 release if the cathode is deeply overcharged. With further increases in temperature, the $LiMn_2O_4$-type spinel structure changes to M_3O_4-type spinel structure with an increased partial TM occupancy at the 8a tetrahedral sites as shown in (Fig. 11d).[123]

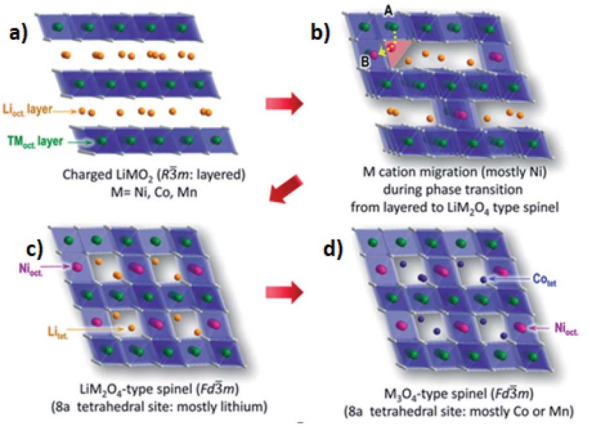

Fig. 11 Schematic illustration of phase transition and the possible TM cation migration path in the charged NMC cathode materials: (a) charged $LiMO_2$ (M = Ni, Co, Mn), (b) M cation migration (mostly Ni), (c) 8a tetrahedral site: mostly Li, (d) 8a tetrahedral site: mostly Co or Mn.[123]

Thermal stability of the charged NCM materials decreases with increasing Ni content but increases with increasing cobalt and manganese content: the more nickel in the composition, the lower the onset temperature of the phase transition, and the sharper the peak of the oxygen release. That means thermal stability may also depend on the compositions of the transition metals. Seong-Min Bak *et al.*[123] have compared the NCM materials NCM433, NCM532, NCM622, and NCM811 by using combined *in situ* time-resolved X-ray diffraction and mass spectroscopy (TR-XRD/MS) techniques, and NCM532 composition could be in good thermal stability due to the well-balanced ratio of nickel to manganese and cobalt. Eunkang Lee *et al.*[134] have also investigated the thermal decomposition process of charged $Li_{0.33}Ni_{0.5+x}Co_{0.2}Mn_{0.3-x}O_2$ (x = 0, 0.1, 0.2) cathode materials by using a combination of synchrotron-based XRD, XAS, and a thermoanalytical DSC technique. Their XRD resulted that the charged Ni-rich NCMs cathodes during the heating process exhibit a larger thermal expansion. Moreover, their XAS results showed that before the onset temperature is reached for the layered to a spinel phase transition, the Ni-ions are reduced, which is related to the formation of oxygen vacancies around Ni-ions. In a charged Ni-rich cathode materials, thermal expansion and oxygen vacancy formation facilitate TM migration and lower the onset temperature of the thermal decomposition reaction by activating an energetically favorable pathway for cation migration. Unfortunately, thermal expansion and oxygen vacancy formation are critical factors that affect the thermal stability of charged Ni-rich NCMs cathode materials.

Huaibin Wang *et al.*[135] have also studied the thermal runaway of NCM111, NCM523, and NCM622 cathode batteries by using Extended Volume Accelerating Rate Calorimeter (EV-ACR). According to this report, the main factors that can trigger the thermal runaway of batteries are O_2 release, lithium plating at the anode, internal short circuit, and the reaction of the cathode with electrolyte. The process from thermal runaway to a fire is mainly contributed by heat generation, accumulation, and propagation.[136] The thermal runaway of LIB goes through nine steps in the EV-ARC test, from low temperature to high temperature,[137] including: (1) high-temperature capacity degradation, (2) SEI film decomposition, (3) anode and electrolyte reaction, (4) separator melting, (5) anode decomposition reaction, (6) electrolyte solution decomposition reaction, (7) binder decomposition reaction, (8) vent and smoke, (9) electrolyte combustion. In the same condition, the thermal runaway also occurs in the LIB modules, which are widely used in electric vehicles and energy storage stations for facing the energy shortage and air pollution, and its thermal runaway is shown in (Fig. 12). Fig. 12a shows a pristine sample cell; (Fig. 12b) shows the components of LIB; in stage II SEI decomposes, Mn is dissolved, and gas is released as shown in (Fig. 12c). In stage III, the separator melt and gas releasing is increased as shown in (Fig. 12d); and in stage IV, the separator is completely broken up

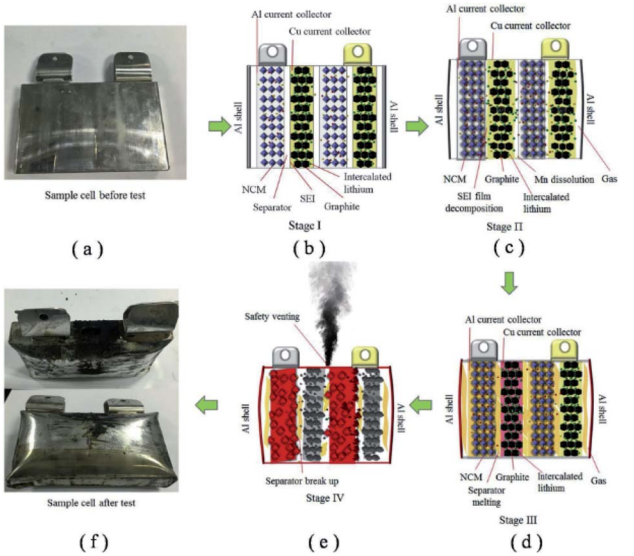

Fig. 12 The thermal runaway mechanism of the LIB modules in EV-ARC tests: (a) sample cell before test, (b) stage I, (c) SEI film decomposition, (d) separate melting, (e) separate break up, (f) sample test after test.[137]

and an internal short circuit is formed causing smoke and explosion of LIB as shown in Fig. 12e and f.

4 Conclusions and future perspectives

In this review, we summarized the surface degradation, mechanical failure and thermal instability of Ni-rich NCM cathode materials for lithium-ion batteries based on the recent findings. The performance degradation and safety hazards are the main problems in Ni-rich NCM cathode material. Performance degradation behaved as declines in capacity and working voltage, and it results from aggressive chemical, structural, and mechanical deterioration, in which there is an increase in volume and impedance of the battery. Because of the thermal instability of Ni-rich NCM materials near fully charged state or at high temperature the safety hazard can occur. This safety hazard is caused by the abuse conditions such as overcharging, overheating and electrical shorting. Li^+/Ni^{2+} cation mixing, particle cracking, phase transformation, electrolyte decomposition, transition metal dissolution, residual lithium compounds, oxygen release, and thermal instabilities are the main problems in Ni-rich cathode active materials. Increasing the upper cut-off voltage can also increase undesirable side reactions at the electrode/electrolyte interface, surface film formation, and metal dissolution, which ultimately decrease the battery lifetime. Commercialization of these cathodes has been proven to be difficult. Hence, further innovations and different state-of-the-art is required to eliminate these issues. Various mitigation strategies such as dopants, gradient layers, surface coatings, carbon matrixes, and advanced synthesis methods proposed by researchers to improve the electrochemical performance of these materials. However, it is very important to understand the degradation mechanisms in order to find effective strategies and to making better batteries. The currently studied degradation mechanisms and the root cause of each challenge in Ni-rich cathode active materials are not widely studied and understood very well. Moreover, the mentioned challenges in this review are also dependent on each other but not extremely identified by scientific investigation. Thus, one degradation mechanism will cause another type of degradation mechanism and the relationship between these degradation mechanisms not studied effectively. Therefore, we recommend that it is good to identify the relationship of each degradation mechanism scientifically and to find a reasonable solution for each challenge to realize the commercialization and high capacity retention of Ni-rich NCM cathode active materials for the next-generation LIBs.

Author contributions

Fikadu Takele Geldasa: writing – original draft. Mesfin Abayneh Kebede: supervision, conceptualization, visualization and editing. Megersa Wodajo Shura: provisioning resources. Fekadu Gashaw Hone: conceptualization, supervision, writing – review and editing.

Conflicts of interest

There are no interest conflicts.

Acknowledgements

We acknowledge Adama Science and Technology University and Oda Bultum University for their financial support.

References

1 S. S. Zhang, *Front. Energy Res.*, 2013, **1**, 1–6.
2 R. Younesi, *Front. Energy Res.*, 2014, **2**, 2013–2014.
3 T. Kåberger, *Global Energy Interconnection*, 2018, **1**, 48–52.
4 B. Scrosat and J. Garche, *J. Power Sources*, 2010, **195**, 2419–2430.
5 J. M. Tarascon and M. Armand, *Nature*, 2001, **414**, 359–367.
6 S. Hwang, D. H. Kim, K. Y. Chung and W. Chang, *Appl. Phys. Lett.*, 2014, **105**, 4.
7 Y. Ding, D. Mu, B. Wu, R. Wang, Z. Zhao and F. Wu, *Appl. Energy*, 2017, **195**, 586–599.
8 W. Cho, S. M. Kim, J. H. Song, T. Yim, S. G. Woo, K. W. Lee, J. S. Kim and Y. J. Kim, *J. Power Sources*, 2015, **282**, 45–50.
9 B. J. Landi, M. J. Ganter, C. D. Cress, R. A. DiLeo and R. P. Raffaelle, *Energy Environ. Sci.*, 2009, **2**, 638–654.
10 S. Liang, W. Yan, X. Wu, Y. Zhang, Y. Zhu, H. Wang and Y. Wu, *Solid State Ionics*, 2018, **318**, 2–18.
11 M. S. Whittingham, *Science*, 1976, **192**, 1126–1127.
12 C. Monroe and J. Newman, *J. Electrochem. Soc.*, 2003, **150**, A1377–A1384.
13 P. C. J. P. J. W. K. Mizushima and J. B. Goodenough, *Jpn. J. Appl. Phys., Part 1*, 2003, **42**, 6131–6134.
14 A. Manthiram, *Nat. Commun.*, 2020, **11**, 1–9.

15 R. Yazami and P. Touzain, *J. Power Sources*, 1983, **9**, 365–371.
16 A. Yoshino, *Angew. Chem., Int. Ed.*, 2012, **51**, 2–5.
17 M. V. Reddy, A. Mauger, C. M. Julien, A. Paolella and K. Zaghib, *Materials*, 2020, **13**, 1884.
18 J. L. Brédas, J. M. Buriak, F. Caruso, K.-Sh. Choi, B. A. Korgel, M. R. Palacín, K. Persson, E. Reichmanis, F. Schüth, R. Seshadri and M. D. Ward, *Chem. Mater.*, 2019, **31**, 8577–8581.
19 Y. Lee, H. Kim, T. Yim, K. Y. Lee and W. Choi, *J. Power Sources*, 2018, **400**, 87–95.
20 W. Shan, S. Huang, H. Zhang and X. Hou, *J. Alloys Compd.*, 2021, **862**, 158022.
21 Y. Lv, X. Cheng, W. Qiang and B. Huang, *J. Power Sources*, 2020, **450**, 227718.
22 J. A. Sanguesa, V. Torres-Sanz, P. Garrido, F. J. Martinez and J. M. Marquez-Barja, *Smart Cities*, 2021, **4**, 372–404.
23 Y. Xia, J. Zheng, C. Wang and M. Gu, *Nano Energy*, 2018, **49**, 434–452.
24 A. O. Said, C. Lee, X. Liu, Z. Wu and S. I. Stoliarov, *Proc. Combust. Inst.*, 2019, **37**, 4173–4180.
25 Q. Liu, X. Su, D. Lei, Y. Qin, J. Wen, F. Guo, Y. A. Wu, Y. Rong, R. Kou, X. Xiao, F. Aguesse, J. Bareño, Y. Ren, W. Lu and Y. Li, *Nat. Energy*, 2018, **3**, 936–943.
26 C. M. Julien, A. Mauger, K. Zaghib and H. Groult, *Inorganics*, 2014, **2**, 132–154.
27 B. Zhu, Z. Yu, L. Meng, Z. Xu, C. Lv, Y. Wang, G. Wei and J. Qu, *Ionics*, 2021, **27**, 2749–2784.
28 X. Chen, Y. Li and J. Wang, *Nanomaterials*, 2021, **11**, 1–9.
29 B. L. Ellis, K. T. Lee and L. F. Nazar, *Chem. Mater.*, 2010, **22**, 691–714.
30 C. Liu, Z. G. Neale and G. Cao, *Mater. Today*, 2016, **19**, 109–123.
31 A. W. Golubkov, D. Fuchs, J. Wagner, H. Wiltsche, C. Stangl, G. Fauler and G. Voitic, *RSC Adv.*, 2014, **4**, 3633.
32 J. P. Pender, G. Jha, D. H. Youn, J. M. Ziegler, I. Andoni, E. J. Choi, A. Heller, B. S. Dunn, P. S. Weiss, R. M. Penner and C. B. Mullins, *ACS Nano*, 2020, **14**, 1243–1295.
33 W. Hua, J. Zhang, Z. Zheng, W. Liu, X. Peng, X. D. Guo, B. Zhong, Y. J. Wang and X. Wang, *Dalton Trans.*, 2014, **43**, 14824–14832.
34 S. K. Jung, H. Gwon, J. Hong, K. Y. Park, D. H. Seo, H. Kim, J. Hyun, W. Yang and K. Kang, *Adv. Energy Mater.*, 2014, **4**, 1–7.
35 H. J. Noh, S. Youn, C. S. Yoon and Y. K. Sun, *J. Power Sources*, 2013, **233**, 121–130.
36 L. De Biasi, A. O. Kondrakov, H. Geßwein, T. Brezesinski, P. Hartmann and J. Janek, *J. Phys. Chem. C*, 2017, **121**, 26163–26171.
37 T. Ohzuku and Y. Makimura, *Chem. Lett.*, 2001, 642–643.
38 Y. Zhu, Y. Huang, R. Du, M. Tang, B. Wang and J. Zhang, *Crystals*, 2021, **11**, 465.
39 P. Zou, Z. Lin, M. Fan, F. Wang, Y. Liu and X. Xiong, *Appl. Surf. Sci.*, 2020, **504**, 144506.
40 S. W. Lee, M. S. Kim, J. H. Jeong, D. H. Kim, K. Y. Chung, K. C. Roh and K. B. Kim, *J. Power Sources*, 2017, **360**, 206–214.
41 L. Wu, X. Tang, X. Chen, Z. Rong, W. Dang, Y. Wang, X. Li, L. Huang and Y. Zhang, *J. Power Sources*, 2020, **445**, 227337.
42 J. Yang, M. Hou, S. Haller, Y. Wang, C. Wang and Y. Xia, *Electrochim. Acta*, 2016, **189**, 101–110.
43 W. Liu, P. Oh, X. Liu, M. J. Lee, W. Cho, S. Chae, Y. Kim and J. Cho, *Angew. Chem., Int. Ed.*, 2015, **54**, 4440–4457.
44 R. Jung, M. Metzger, F. Maglia, C. Stinner and H. A. Gasteiger, *J. Electrochem. Soc.*, 2017, **164**, A1361–A1377.
45 I. Buchberger, S. Seidlmayer, A. Pokharel, M. Piana, J. Hattendorff, P. Kudejova, R. Gilles and H. A. Gasteiger, *J. Electrochem. Soc.*, 2015, **162**, A2737–A2746.
46 B. Strehle, K. Kleiner, R. Jung, F. Chesneau, M. Mendez, H. A. Gasteiger and M. Piana, *J. Electrochem. Soc.*, 2017, **164**, A400–A406.
47 Y. Ruan, X. Song, Y. Fu, C. Song and V. Battaglia, *J. Power Sources*, 2018, **400**, 539–548.
48 H. H. Sun, H. H. Ryu, U. H. Kim, J. A. Weeks, A. Heller, Y. K. Sun and C. B. Mullins, *ACS Energy Lett.*, 2020, **5**, 1136–1146.
49 X. Cheng, J. Zheng, J. Lu, Y. Li, P. Yan and Y. Zhang, *Nano Energy*, 2019, **62**, 30–37.
50 J. S. Edge, S. O'Kane, R. Prosser, N. D. Kirkaldy, A. N. Patel, A. Hales, A. Ghosh, W. Ai, J. Chen, J. Yang, S. Li, M.-C. Pang, L. Bravo Diaz, A. Tomaszewska, M. Waseem Marzook, K. N. Radhakrishnan, H. Wang, Y. Patel, B. Wu and G. J. Offer, *Phys. Chem. Chem. Phys.*, 2021, **23**, 8200.
51 R. S. Arumugam, L. Ma, J. Li, X. Xia, J. M. Paulsen and J. R. Dahn, *J. Electrochem. Soc.*, 2016, **163**, A2531–A2538.
52 J. Wandt, A. T. S. Freiberg, A. Ogrodnik and H. A. Gasteiger, *Mater. Today*, 2018, **21**, 825–833.
53 P. Pang, X. Tan, Z. Wang, Z. Cai, J. Nan, Z. Xing and H. Li, *Electrochim. Acta*, 2021, **365**, 137380.
54 H. H. Sun and A. Manthiram, *Chem. Mater.*, 2017, **29**, 8486–8493.
55 S. S. Jan, S. Nurgul, X. Shi, H. Xia and H. Pang, *Electrochim. Acta*, 2014, **149**, 86–93.
56 H. Yu, Y. Qian, M. Otani, D. Tang, S. Guo, Y. Zhu and H. Zhou, *Energy Environ. Sci.*, 2014, **7**, 1068–1078.
57 T. He, L. Chen, Y. Su, Y. Lu, L. Bao, G. Chen, Q. Zhang, S. Chen and F. Wu, *J. Power Sources*, 2019, **441**, 227195.
58 J. Zheng and F. Wang, *Acc. Chem. Res.*, 2019, **52**, 2201–2209.
59 C. Liang, R. C. Longo, F. Kong, C. Zhang, Y. Nie, Y. Zheng, J. S. Kim, S. Jeon, S. A. Choi and K. Cho, *J. Power Sources*, 2017, **340**, 217–228.
60 X. Yao, Z. Xu, Z. Yao, W. Cheng, H. Gao, Q. Zhao, J. Li and A. Zhou, *Mater. Today Commun.*, 2019, **19**, 262–270.
61 J. Zheng, P. Yan, L. Estevez, C. Wang and J. G. Zhang, *Nano Energy*, 2018, **49**, 538–548.
62 Y. C. Li, W. Xiang, Y. Xiao, Z. G. Wu, C. L. Xu, W. Xu, Y. D. Xu, C. Wu, Z. G. Yang and X. D. Guo, *J. Power Sources*, 2019, **423**, 144–151.
63 H. Ronduda, M. Zybert, A. Szczęsna-Chrzan, T. Trzeciak, A. Ostrowski, D. Szymański, W. Wieczorek, W. Raróg-Pilecka and M. Marcinek, *Nanomaterials*, 2020, **10**, 1–21.
64 P. Li, S. Zhao, Y. Zhuang, J. Adkins, Q. Zhou and J. Zheng, *Appl. Surf. Sci.*, 2018, **453**, 93–100.

65 F. Wu, J. Tian, Y. Su, J. Wang, C. Zhang, L. Bao, T. He, J. Li and S. Chen, *ACS Appl. Mater. Interfaces*, 2015, **7**, 7702–7708.
66 B. Huang, M. Wang, X. Zhang, Z. Zhao, L. Chen and Y. Gu, *J. Alloys Compd.*, 2020, **830**, 154619.
67 U. H. Kim, J. H. Kim, J. Y. Hwang, H. H. Ryu, C. S. Yoon and Y. K. Sun, *Mater. Today*, 2019, **23**, 26–36.
68 R. Wang, G. Qian, T. Liu, M. Li, J. Liu, B. Zhang, W. Zhu, S. Li, W. Zhao, W. Yang, X. Ma, Z. Fu, Y. Liu, J. Yang, L. Jin, Y. Xiao and F. Pan, *Nano Energy*, 2019, **62**, 709–717.
69 J. Zheng, P. Yan, J. Zhang, M. H. Engelhard, Z. Zhu, B. J. Polzin, S. Trask, J. Xiao, C. Wang and J. Zhang, *Nano Res.*, 2017, **10**, 4221–4231.
70 W. Liu, P. Oh, X. Liu, M. J. Lee, W. Cho, S. Chae, Y. Kim and J. Cho, *Angew. Chem., Int. Ed.*, 2015, **54**, 4440–4457.
71 H.-H. Ryu, B. Namkoong, J.-H. Kim, I. Belharouak, C. S. Yoon and Y.-K. Sun, *ACS Energy Lett.*, 2021, **6**, 2726–2734.
72 X. Zhao, L. An, J. Sun and G. Liang, *J. Electroanal. Chem.*, 2018, **810**, 1–10.
73 S. S. Zhang, *Energy Storage Mater.*, 2020, **24**, 247–254.
74 J. Chen, H. Yang, T. Li, C. Liu, H. Tong, J. Chen, Z. Liu, L. Xia, Z. Chen, J. Duan and L. Li, *Front. Chem.*, 2019, **7**, 1–10.
75 Y. Liu, L. b. Tang, H. x. Wei, X. h. Zhang, Z. j. He, Y. j. Li and J. c. Zheng, *Nano Energy*, 2019, **65**, 104043.
76 C. Fu, G. Li, D. Luo, Q. Li, J. Fan and L. Li, *ACS Appl. Mater. Interfaces*, 2014, **6**, 15822–15831.
77 P. He, H. Yu, D. Li and H. Zhou, *J. Mater. Chem.*, 2012, **22**, 3680–3695.
78 G. Qian, Y. Zhang, L. Li, R. Zhang, J. Xu, Z. Cheng, S. Xie, H. Wang, Q. Rao, Y. He, Y. Shen, L. Chen, M. Tang and Z. F. Ma, *Energy Storage Mater.*, 2020, **27**, 140–149.
79 S. Hwang, E. Jo, K. Y. Chung, K. S. Hwang, S. M. Kim and W. Chang, *J. Phys. Chem. Lett.*, 2017, **8**, 5758–5763.
80 X. Fan, Y. Liu, X. Ou, J. Zhang, B. Zhang, D. Wang and G. Hu, *Chem. Eng. J.*, 2020, **393**, 124709.
81 H. Jia, W. Zhu, Z. Xu, X. Nie, T. Liu, L. Gao and J. Zhao, *Electrochim. Acta*, 2018, **266**, 7–16.
82 F. Lin, I. M. Markus, D. Nordlund, T. C. Weng, M. D. Asta, H. L. Xin and M. M. Doeff, *Nat. Commun.*, 2014, **5**, 3529.
83 F. Wu, N. Liu, L. Chen, Y. Su, G. Tan, L. Bao, Q. Zhang, Y. Lu, J. Wang, S. Chen and J. Tan, *Nano Energy*, 2019, **59**, 50–57.
84 H. Yu, Y. G. So, A. Kuwabara, E. Tochigi, N. Shibata, T. Kudo, H. Zhou and Y. Ikuhara, *Nano Lett.*, 2016, **16**, 2907–2915.
85 C. Xu, W. Xiang, Z. Wu, Y. Xu, Y. Li, Y. Wang, Y. Xiao, X. Guo and B. Zhong, *ACS Appl. Mater. Interfaces*, 2019, **11**, 16629–16638.
86 L. Zou, W. Zhao, Z. Liu, H. Jia, J. Zheng, G. Wang, Y. Yang, J. G. Zhang and C. Wang, *ACS Energy Lett.*, 2018, **3**, 2433–2440.
87 S. M. Bak, K. W. Nam, W. Chang, X. Yu, E. Hu, S. Hwang, E. A. Stach, K. B. Kim, K. Y. Chung and X. Q. Yang, *Chem. Mater.*, 2013, **25**, 337–351.
88 X. Yang, Y. Tang, J. Zheng, G. Shang, J. Wu, Y. Lai, J. Li and Z. Zhang, *Electrochim. Acta*, 2019, **320**, 134587.
89 Y. Su, Y. Yang, L. Chen, Y. Lu, L. Bao, G. Chen, Z. Yang, Q. Zhang, J. Wang, R. Chen, S. Chen and F. Wu, *Electrochim. Acta*, 2018, **292**, 217–226.
90 S. Oswald, D. Pritzl, M. Wetjen and H. A. Gasteiger, *J. Electrochem. Soc.*, 2020, **167**, 100511.
91 R. Ning, K. Yuan, K. Zhang, C. Shen and K. Xie, *Appl. Surf. Sci.*, 2021, **542**, 148663.
92 K. Edström, T. Gustafsson and J. O. Thomas, *Electrochim. Acta*, 2004, **50**, 397–403.
93 J. M. Lim, T. Hwang, D. Kim, M. S. Park, K. Cho and M. Cho, *Sci. Rep.*, 2017, **7**, 2–11.
94 I. Takahashi, H. Kiuchi, A. Ohma, T. Fukunaga and E. Matsubara, *J. Phys. Chem. C*, 2020, **124**, 9243–9248.
95 H. H. Ryu, N. Y. Park, T. C. Noh, G. C. Kang, F. Maglia, S. J. Kim, C. S. Yoon and Y. K. Sun, *ACS Energy Lett.*, 2021, **6**, 216–223.
96 S. Schweidler, L. De Biasi, G. Garcia, A. Mazilkin, P. Hartmann, T. Brezesinski and J. Janek, *ACS Appl. Energy Mater.*, 2019, **2**, 7375–7384.
97 S.-M. Bak, K. W. Nam, W. Chang, X. Yu, E. Hu, S. Hwang, E. A. Stach, K. B. Kim, K. Y. Chung and X. Q. Yang, *Chem. Mater.*, 2013, **25**, 337–351.
98 W. Li, X. Liu, H. Celio, P. Smith, A. Dolocan, M. Chi and A. Manthiram, *Adv. Energy Mater.*, 2018, **8**, 1703154.
99 S. J. Sim, S. H. Lee, B. S. Jin and H. S. Kim, *J. Power Sources*, 2021, **481**, 229037.
100 S. Gao, X. Zhan and Y. T. Cheng, *J. Power Sources*, 2019, **410**, 45–52.
101 W. Tang, Z. Chen, F. Xiong, F. Chen, C. Huang, Q. Gao, T. Wang, Z. Yang and W. Zhang, *J. Power Sources*, 2019, **412**, 246–254.
102 H. J. Song, S. H. Jang, J. Ahn, S. H. Oh and T. Yim, *J. Power Sources*, 2019, **416**, 1–8.
103 Z. Gan, G. Hu, Z. Peng, Y. Cao, H. Tong and K. Du, *Appl. Surf. Sci.*, 2019, **481**, 1228–1238.
104 Z. Ruff, C. Xu and C. P. Grey, *J. Electrochem. Soc.*, 2021, **168**, 060518.
105 H. Ji, S. Ho, Y. Lee, J. Kim and T. Yim, *J. Power Sources*, 2021, **483**, 229218.
106 K. Ishidzu, Y. Oka and T. Nakamura, *Solid State Ionics*, 2016, **288**, 176–179.
107 D. S. Ko, J. H. Park, S. Park, Y. N. Ham, S. J. Ahn, J. H. Park, H. N. Han, E. Lee, W. S. Jeon and C. Jung, *Nano Energy*, 2019, **56**, 434–442.
108 J. Wandt, A. Freiberg, R. Thomas, Y. Gorlin, A. Siebel, R. Jung, H. A. Gasteiger and M. Tromp, *J. Mater. Chem. A*, 2016, **4**, 18300–18305.
109 Y. Ding, D. Mu, B. Wu, Z. Zhao and R. Wang, *Ceram. Int.*, 2020, **46**, 9436–9445.
110 Y. Su, L. Li, G. Chen, L. Chen, N. Li, Y. Lu, L. Bao, S. Chen and F. Wu, *Chin. J. Chem.*, 2021, **39**, 189–198.
111 D.-H. Cho, C.-H. Jo, W. Cho, Y.-J. Kim, H. Yashiro, Y.-K. Sun and S.-T. Myung, *J. Electrochem. Soc.*, 2014, **161**, A920–A926.
112 P. Sun, F. Du, Q. Zhou, D. Hu, T. Xu, C. Mei, Q. Hao, Z. Fan and J. Zheng, *J. Power Sources*, 2021, **495**, 229761.
113 J. Kim, H. Lee, H. Cha, M. Yoon, M. Park and J. Cho, *Adv. Energy Mater.*, 2018, **8**, 1810023.

114 Y. Zou, X. Yang, C. Lv, T. Liu, Y. Xia, L. Shang, G. I. N. Waterhouse, D. Yang and T. Zhang, *Adv. Sci.*, 2017, **4**, 1–8.
115 S. W. Doo, S. Lee, H. Kim, J. H. Choi and K. T. Lee, *ACS Appl. Energy Mater.*, 2019, **2**, 6246–6253.
116 J. H. Park, B. Choi, Y. S. Kang, S. Y. Park, D. J. Yun, I. Park, J. H. Shim, J. H. Park, H. N. Han and K. Park, *Energy Technol.*, 2018, **6**, 1361–1369.
117 T. Chen, X. Li, H. Wang, X. Yan, L. Wang, B. Deng, W. Ge and M. Qu, *J. Power Sources*, 2018, **374**, 1–11.
118 Y. You, H. Celio, J. Li, A. Dolocan and A. Manthiram, *Angew. Chem., Int. Ed.*, 2018, **57**, 6480–6485.
119 V. C. Ho, S. Jeong, T. Yim and J. Mun, *J. Power Sources*, 2020, **450**, 227625.
120 S. Sharifi-Asl, J. Lu, K. Amine and R. Shahbazian-Yassar, *Adv. Energy Mater.*, 2019, **9**, 1–19.
121 T. Cai, A. G. Stefanopoulou and J. B. Siegel, *J. Electrochem. Soc.*, 2019, **166**, A2431–A2443.
122 M. Kaliaperumal, M. S. Dharanendrakumar, S. Prasanna, K. V. Abhishek, R. K. Chidambaram, S. Adams, K. Zaghib and M. V. Reddy, *Materials*, 2021, **14**, 5676.
123 S.-m. Bak, E. Hu, Y. Zhou, X. Yu, S. D. Senanayake, S.-j. Cho, K.-b. Kim, K. Y. Chung, X.-q. Yang and K.-w. Nam, *ACS Appl. Mater. Interfaces*, 2014, **6**, 22594–22601.
124 S. Ahmed, A. Pokle, S. Schweidler, A. Beyer, M. Bianchini, F. Walther, A. Mazilkin, P. Hartmann, T. Brezesinski, J. Janek and K. Volz, *ACS Nano*, 2019, **13**, 10694–10704.
125 C. Mao, R. E. Ruther, L. Geng, Z. Li, D. N. Leonard, H. M. Meyer, R. L. Sacci and D. L. Wood, *ACS Appl. Mater. Interfaces*, 2019, **11**, 43235–43243.
126 H. Zhang, B. M. May, F. Omenya, M. S. Whittingham, J. Cabana and G. Zhou, *Chem. Mater.*, 2019, **31**, 7790–7798.
127 K. Min, S. W. Seo, Y. Y. Song, H. S. Lee and E. Cho, *Phys. Chem. Chem. Phys.*, 2017, **19**, 1762–1769.
128 R. Jung, M. Metzger, F. Maglia, C. Stinner and H. A. Gasteiger, *J. Phys. Chem. Lett.*, 2017, **8**, 4820–4825.
129 E. J. Lee, Z. Chen, H. J. Noh, S. C. Nam, S. Kang, D. H. Kim, K. Amine and Y. K. Sun, *Nano Lett.*, 2014, **14**, 4873–4880.
130 R. Jung, P. Strobl, F. Maglia, C. Stinner and H. A. Gasteiger, *J. Electrochem. Soc.*, 2018, **165**, 2869–2879.
131 T. Hatsukade, A. Schiele, P. Hartmann, T. Brezesinski and J. Janek, *ACS Appl. Mater. Interfaces*, 2018, **10**, 38892–38899.
132 D. Pritzl, T. Teufl, A. T. S. Freiberg, B. Strehle, J. Sicklinger, H. Sommer, P. Hartmann and H. A. Gasteiger, *J. Electrochem. Soc.*, 2019, **166**, A4056–A4066.
133 Y. Huang, Y. C. Lin, D. M. Jenkins, N. A. Chernova, Y. Chung, B. Radhakrishnan, I. H. Chu, J. Fang, Q. Wang, F. Omenya, S. P. Ong and M. S. Whittingham, *ACS Appl. Mater. Interfaces*, 2016, **8**, 7013–7021.
134 E. Lee, S. Muhammad, T. Kim, H. Kim, W. Lee and W. S. Yoon, *Adv. Sci.*, 2020, **7**, 1–12.
135 H. Wang, Z. Du, X. Rui, S. Wang, C. Jin, L. He, F. Zhang, Q. Wang and X. Feng, *J. Hazard. Mater.*, 2020, **393**, 122361.
136 M. Chen, O. Dongxu, J. Liu and J. Wang, *Appl. Therm. Eng.*, 2019, **157**, 113750.
137 H. Li, Q. Duan, C. Zhao, Z. Huang and Q. Wang, *J. Hazard. Mater.*, 2019, **375**, 241–254.